Near-Ground Wind Profiles of Tornadic and Nontornadic Environments in the United States and Europe from ERA5 Reanalyses

BRICE E. COFFER, MATEUSZ TASZAREK, b,c AND MATTHEW D. PARKER

^a Department of Marine, Earth, and Atmospheric Sciences, North Carolina State University, Raleigh, North Carolina

^b Department of Meteorology and Climatology, Adam Mickiewicz University, Poznań, Poland

^c National Severe Storms Laboratory, Norman, Oklahoma

(Manuscript received 27 August 2020, in final form 16 October 2020)

ABSTRACT: The near-ground wind profile exhibits significant control over the organization, intensity, and steadiness of low-level updrafts and mesocyclones in severe thunderstorms, and thus their probability of being associated with tornadogenesis. The present work builds upon recent improvements in supercell tornado forecasting by examining the possibility that storm-relative helicity (SRH) integrated over progressively shallower layers has increased skill in differentiating between significantly tornadic and nontornadic severe thunderstorms. For a population of severe thunderstorms in the United States and Europe, sounding-derived parameters are computed from the ERA5 reanalysis, which has significantly enhanced vertical resolution compared to prior analyses. The ERA5 is shown to represent U.S. convective environments similarly to the Storm Prediction Center's mesoscale surface objective analysis, but its greater number of vertical levels in the lower troposphere permits calculations to be performed over shallower layers. In the ERA5, progressively shallower layers of SRH provide greater discrimination between nontornadic and significantly tornadic thunderstorms in both the United States and Europe. In the United States, the 0–100 m AGL layer has the highest forecast skill of any SRH layer tested, although gains are comparatively modest for layers shallower than 0–500 m AGL. In Europe, the benefit from using shallower layers of SRH is even greater; the lower-tropospheric SRH is by far the most skillful ingredient there, far exceeding related composite parameters like the significant tornado parameter (which has negligible skill in Europe).

KEYWORDS: Europe; Wind shear; Severe storms; Supercells; Tornadoes; Mesoscale forecasting

1. Introduction

The ability to forecast severe thunderstorms, and specifically tornadic supercells, has improved dramatically over recent decades. In the United States, operationally useful outlooks are often issued several days in advance of high-end tornado outbreaks. Much of this progress can be attributed to increased understanding of the environmental controls on tornado formation through numerical modeling experiments, as well as the collection of severe thunderstorm proximity soundings (both balloon-borne radiosondes and vertical profiles extracted from model analyses). Proximity soundings have highlighted ingredients fundamental to severe weather forecasting, including conditional instability, low-level relative humidity, and vertical wind shear (Beebe 1958; Maddox 1976; Schaefer and Livingston 1988; Davies and Johns 1993; Johns et al. 1993; Brooks et al. 1994; Kerr and Darkow 1996; Rasmussen and Blanchard 1998; Rasmussen 2003; Thompson et al. 2003; Craven et al. 2004). In particular, the vertical wind profile has a profound effect on the development, maintenance, and organization of thunderstorms (Chisholm and Renick 1972; Weisman and Klemp 1982; Warren et al. 2017; Peters et al. 2019), with highly streamwise horizontal vorticity concentrated in the lower troposphere being notably favorable for tornadic supercells (Davies-Jones 1984; Markowski et al. 2003; Esterheld and Giuliano 2008; Parker 2014; Wade et al. 2018; Coffer et al. 2019, hereafter C19).

The gold standard in the United States for model-based proximity soundings are vertical profiles extracted from the

Corresponding author: Brice Coffer, becoffer@ncsu.edu

Storm Prediction Center's (SPC) mesoscale surface objective analysis (SFCOA; Bothwell et al. 2002), which currently uses the Rapid Refresh (RAP; Benjamin et al. 2016), and prior to May 2012, used the Rapid Update Cycle (RUC; Benjamin et al. 2004), as its background environment. These proximity soundings have been used extensively in the development of the significant tornado parameter (STP), which is a multiple ingredient, composite index combining forecasting proxies that are known to be favorable for supercell thunderstorms and specifically tornadic supercells (Thompson et al. 2003, 2007, 2012).

A key component of the STP is the lower-tropospheric storm-relative helicity (SRH), which has traditionally been calculated over the depths that approximate the inflow layer into a mature, right-moving supercell, approximately 1–3 km above ground level (AGL). However, in composite near-storm profiles from Parker (2014), the near-ground wind profile was the most noticeable environmental difference between nontornadic and tornadic supercells during the Verification of the Origins of Rotation in Tornadoes Experiment (VORTEX2; Wurman et al. 2012). While the 0–3 km AGL SRH was slightly lower in the tornadic VORTEX2 composite compared to the nontornadic (330 versus 360 m² s⁻²), the 0–500 m AGL SRH was twice as high in the tornadic VORTEX2 composite than the nontornadic (159 versus 80 m² s⁻²). In simulations based on the Parker (2014) composite nontornadic supercell sounding,

¹ Hereafter, vertical profiles extracted from the SPC RUC/RAP SFCOA will be referred simply as SFCOA. See Table 1 for a complete list of acronyms used throughout in this paper.

Coffer and Parker (2017, 2018) found near-ground crosswise horizontal vorticity to be unfavorable for steady low-level mesocylones and thus tornadogenesis. These results led C19 to focus on the forecast skill of a particular component of the STP, the lower-tropospheric SRH, specifically asking whether progressively shallower layers of SRH would lead to increased forecast skill compared to the deeper layers typically used in operations. SRH integrated through the 0–500 m AGL layer led to the greatest discrimination between significantly tornadic and nontornadic supercells. However, due to the vertical resolution of the SFCOA dataset used in C19, even shallower layers could not be reliably explored.

In contrast to the multitude of convective environments studies in the United States over the past decades, similar investigations across Europe have long been hindered by a lack of standardized reporting practices of severe weather events. To address this issue, researchers at the European Severe Storms Laboratory (ESSL) began developing the European severe weather database (ESWD) in the mid-2000s to create a standardized database across nations in collaboration with networks of volunteers and multiple meteorological agencies (Dotzek et al. 2009). Historical and current reports are actively integrated into the ESWD and recent events are continuously quality controlled (Groenemeijer and Kühne 2014). The creation of ESWD has enabled proximity sounding studies and other forecast evaluations of severe weather environments in Europe (e.g., Púčik et al. 2015; Taszarek et al. 2017, 2019, 2020b). Some unavoidable limitations of this past work have been the spatial and temporal availability of the proximity soundings, both in observations and model-based vertical profiles. Balloon-borne radiosondes are most often taken at select locations twice per day (0000-1200 UTC), neither of which are at the climatological maximum of tornado frequency in Europe. Thus, broad proximity criteria are necessary to have a sufficient sample size. Meanwhile, model-based proximity soundings studies have typically relied on coarser global analyses/reanalysis datasets (e.g., Brooks 2009; Kaltenböck et al. 2009; Taszarek et al. 2020b), which often struggle to represent the mesoscale complexity of severe thunderstorm environments (King and Kennedy 2019).

In 2019 the European Centre for Medium-Range Weather Forecasting (ECMWF) began publicly releasing the fifth iteration of their global reanalysis, the ERA5. In addition to a decade of developments in model physics, core dynamics, and data assimilation, the ERA5 has significantly enhanced horizontal grid spacing (31 km compared to 80 km in the previous generation) and hourly output instead of every 6 h (Hersbach et al. 2020). The ERA5 also has significantly more vertical levels than prior reanalyses with 137 model levels from the surface up to a height of 80 km. Of particular interest to severe thunderstorm forecasting, in the lowest 500 m AGL of the atmosphere, the ERA5 has an order of magnitude more grid points than the SFCOA (approximately 14 in the ERA5 versus 3 in the SFCOA). More resolution in the planetary boundary layer (PBL) means a more faithful representation of the input observations, as well as better retention of shallow features in the output analysis. In fact, validation over millions of observed soundings in North America and Europe reveals the

TABLE 1. List of acronyms.

Acronym	Definition			
AGL	Above ground level			
CAPE	Convective available potential energy			
CIN	Convective inhibition			
CSI	Critical success index			
EBWD	Effective bulk wind difference			
ECMWF	European Centre for Medium-Range Weather			
	Forecasting			
ERA5	Fifth major global reanalysis produced by ECMWF			
ESSL	European Severe Storms Labratory			
ESWD	European Severe Weather Database			
FAR	False alarm ratio			
LCL	Lifted condensation layer			
ML	Mixed layer (100 hPa)			
MAD	Mean absolute deviation			
PBL	Planetary boundary layer			
POD	Probability of detection			
POFD	Probability of false detection			
RAP	Rapid Refresh			
RUC	Rapid Update Cycle			
SFCOA	SPC mesoscale surface objective analysis			
SPC	Storm Prediction Center			
SRH	Storm-relative helicity			
STP	Significant tornado parameter			
TSS	True skill score			

ERA5 to be the best currently available global reanalysis in representing convective environments (Taszarek et al. 2020c, manuscript submitted to *J. Climate*). Considering some of the limitations of model-based proximity soundings in both the United States and in Europe, this new dataset has the potential to address questions not possible in previous studies (e.g., Li et al. 2020; Taszarek et al. 2020a,b).

The purpose of this study is to extend the work of C19 to even shallower layers of SRH integration that are represented well in the ERA5 (but not in the SFCOA) and to see whether near-ground SRH and the STP differentiate between non-tornadic and tornadic thunderstorm environments across Europe as well as they do in the United States.

Specifically, this paper addresses the following three questions:

- 1) Does the ERA5 faithfully represent severe weather environments in the United States compared to the SFCOA?
- 2) Do even shallower layers of SRH than 0-500 m AGL have increased forecast skill for significant tornadoes in severe, right-moving supercells in the United States?
- 3) Do the near-ground wind profile and severe weather composite parameters, such as the STP, show similar skill in European tornadic events?

Section 2 describes the SFCOA and ERA5 datasets in more detail. Section 3 shows comparisons between those two datasets for severe supercells in the United States and provides additional analysis of differences in the near-ground wind profile between significantly tornadic and nontornadic supercells. Lessons learned from the U.S. dataset are then be applied to European severe weather reports in section 4.

2. Methods

The U.S. severe weather events are the same population as in C19, drawn from the SPC convective mode database described by Smith et al. (2012) and Thompson et al. (2012). In short, the U.S. dataset is exclusively comprised of severe, rightmoving supercells, including 9355 tornadoes (1612 of which are significantly tornadic), 3788 severe wind reports, and 7051 severe hail events (Fig. 1a). Environmental base-state data corresponding to each severe report are obtained from archived vertical profiles from the SPC's SFCOA. Notable to the current work, these data are provided on isobaric levels with 25-hPa vertical resolution (e.g., 1000, 975, 950, 925 hPa, etc.). The use of isobaric data implies limited vertical resolution near the ground. On the native hybrid sigma-isentropic coordinate system, the SFCOA has roughly nine levels in the lowest kilometer (six below 500 m AGL) versus five levels (three below 500 m AGL) on the isobaric grids through the same depth. Shallower layers of SRH integration than 500 m AGL could not be reliably tested in C19 because layers below 250 m AGL might only consist of one unique data point.

The European severe weather events are taken from the ESWD from the years 1979 to 2019 (QC0+, QC1, and QC2 quality reports), corresponding to the availability of ERA5 data at this time. A more detailed description of the ESWD was provided by Dotzek et al. (2009) and Groenemeijer and Kühne (2014). Because comprehensive convective mode labels are not available for the European events, only the ESWD hazard types of "tornadoes" and "large hail" are considered to facilitate a natural comparison to the exclusively supercell events of the U.S. dataset. To further refine the nontornadic subset to probable supercell events, the "large hail" category is narrowed down to solely significantly severe hail reports greater than 5 cm (~2 in.), since, at least in the United States, supercells produce the vast majority of such hail reports (Rasmussen and Blanchard 1998; Smith et al. 2012; Blair et al. 2017). Finally, tornado events occurring over a water surface (i.e., waterspouts) with an F0 rating are removed, although it is possible that, during the report collection process, this water surface label is not always correctly applied to some tornadoes that form over water and move onshore (specifically the Spanish Balearic Islands and along the Italian coast stand out as a possibility from Fig. 1b).

The resulting list of European severe weather reports are spatiotemporally filtered, using a spatial threshold of 75 km and a time window of 120 min. For a given time and space window, only the highest magnitude report was kept. This is similar to the filtering procedure for the U.S. severe weather events and helps ensure each report is in a unique environment relative to similar reports in space/time. Last, profiles were discarded if they contained less than $10\,\mathrm{J\,kg^{-1}}$ in MLCAPE.²

These profiles were assumed to be unrepresentative of the actual conditions for that report. In total, for Europe, this results in 3539 tornadoes (479 of which are significantly tornadic) and 1247 significantly severe hail events (169 of which are larger than 8 cm in diameter; Fig. 1b).

Vertical profiles of pressure, height, temperature, dewpoint temperature, and both horizontal wind components are extracted for each report (United States and Europe) at the nearest ERA5 grid point and at the closest hourly analysis time. Derived parameters (e.g., CAPE, SRH, STP) for each vertical profile are independently calculated from the gridpoint sounding (as opposed to using the provided values directly from the ERA5). Forecast skill for those parameters are compared against one another using a classic 2 × 2 contingency table (Doswell et al. 1990; Doswell and Schultz 2006). As in C19, the true skill statistic (TSS, also known as the Pierce Skill Score; Wilks 2011, chapter 8) is the main metric used herein to evaluate forecast skill between the sounding-derived parameters. The TSS highlights parameters that maximize probability of detection (POD; or "hit rate") while minimizing probability of false detection (POFD; or "false alarm rate"). For completeness, in addition to TSS, performance diagrams (Roebber 2009) showing POD, false alarm ratio (FAR), bias, and critical success index (CSI) are also presented for key layers of SRH integration.

3. United States

a. Comparing the ERA5 to the SFCOA

Significant advances in our understanding of the environmental controls on tornado formation occurred once numerical weather models had sufficient resolution and data assimilation capabilities to depict mesoscale features of interest, starting with the ETA model in the 1990s (Thompson 1998) and progressing to the RUC and eventually the RAP models that underpin the SFCOA. Proximity soundings from these models have become the standard for representing severe weather environments in the United States and are often considered the benchmark for assessing other global reanalysis datasets' ability to represent convective environments (King and Kennedy 2019), despite some known biases (Thompson et al. 2003; Coniglio 2012). Therefore, before using the ERA5 reanalysis to assess near-ground wind profiles for supercell environments in the United States, it is first worthwhile to compare the ERA5 to the SFCOA.

The ERA5 reanalysis is compared to the SFCOA proximity soundings from C19 for each of the five components of the effective-layer significant tornado parameter (STP; Thompson et al. 2003, 2007) using the 0–500 m AGL SRH (STP500; C19). These components include the mixed-layer (ML; lowest 100 hPa) convective available potential energy (MLCAPE), convective inhibition (MLCIN), and height of the lifted condensation level (MLLCL), the effective bulk wind difference (EBWD; Thompson et al. 2007), and the 0–500 m AGL SRH (SRH500). The formulation of the STP500 is

 $^{^2}$ The general conclusions of this article were largely insensitive to a minimum MLCAPE threshold of 0, 10, or $50\,\mathrm{J\,K^{-1}}$ (or even no threshold at all), likely because the vast majority (~85%) of the profiles with no buoyancy were weakly tornadic events (F0–F1) and much of the analysis hereafter focuses on significantly tornadic versus nontornadic thunderstorm environments. Nevertheless, eliminating lower CAPE European severe weather events from this study may introduce a small bias with respect to low-topped thunderstorms.

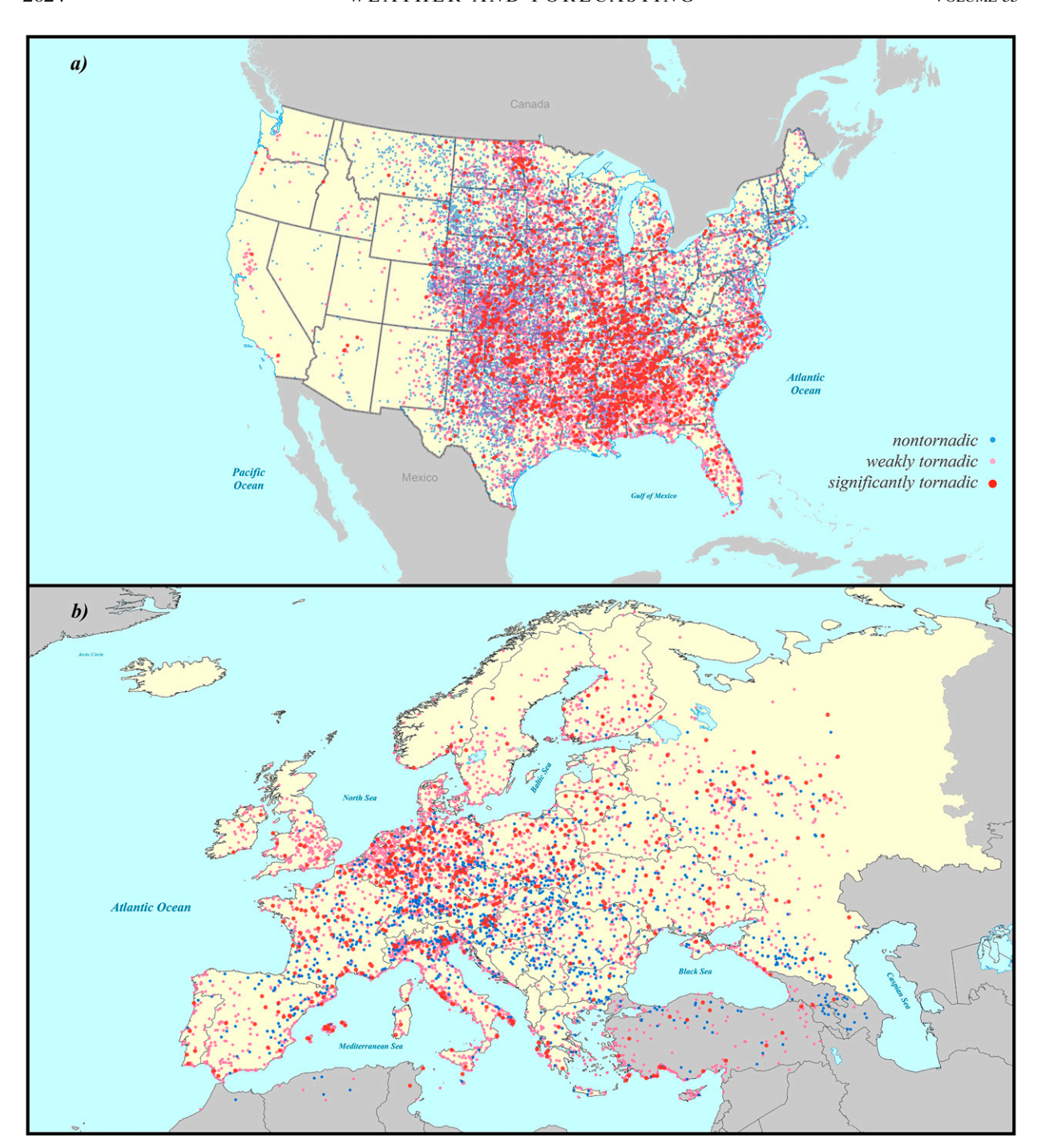


FIG. 1. (a) Map of all right-moving supercell events in the United States from Coffer et al. (2019) during the years 2005–17, separated by significant tornadoes [(E)F2+; red], weak tornadoes [(E)F0–1; pink], and severe nontornadic storms (blue). The continental United States is highlighted in beige. (b) Map of significantly severe hail and tornado reports from the European Severe Weather Database (ESWD) during the years 1979–2019. Plotting conventions for reports are as in (a). "Geographic" Europe is highlighted in beige, although ESWD collects reports elsewhere (e.g., northwest Africa and the Anatolia peninsula of Turkey). Both panels use the 1984 World Geodetic System (WGS) with a Robinson projection at 1:17 000 000.

STP500 components in the SFCOA and ERA5: USA

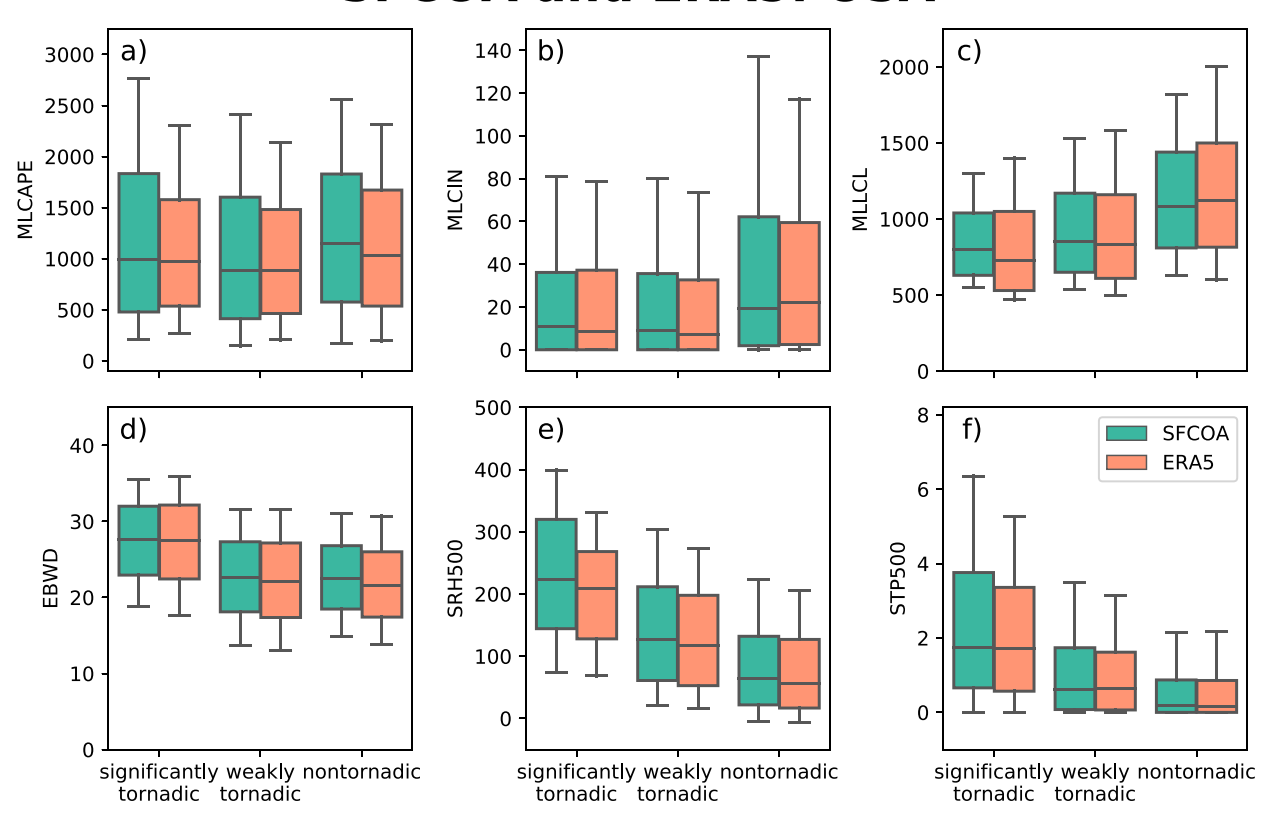


FIG. 2. Box-and-whisker plots of each component of the effective-layer significant tornado parameter (STP) using the $0-500\,\mathrm{m}$ AGL SRH (SRH500; $\mathrm{m^2\,s^{-2}}$) for all right-moving supercell events, separated by significant tornadoes [(E)F2+], n=1612, weak tornadoes [(E)F0-1, n=7743], and nontornadic severe supercells (n=10839) from both the SFCOA (green) from Coffer et al. (2019) and in the ERA5 (orange). The components are as follows: (a) mixed-layer convective available potential energy (MLCAPE), (b) mixed-layer convective inhibition (MLCIN), (c) mixed-layer lifted condensation level (MLLCL), (d) effective bulk wind difference (EBWD), and (e) SRH500. (f) The resulting distributions of the STP500 composite parameter. The whiskers extend upward to the 90th and downward to the 10th percentiles. Outliers are excluded for clarity.

$$\begin{split} \text{STP500} &= \frac{\text{MLCAPE}}{1500\,\text{J}\,\text{kg}^{-1}} \times \frac{2000 - \text{MLLCL}}{1000\,\text{m}} \times \frac{200 + \text{MLCIN}}{150\,\text{J}\,\text{kg}^{-1}} \\ &\times \frac{\text{EBWD}}{20\,\text{m}\,\text{s}^{-1}} \times \frac{\text{SRH500}}{75\,\text{m}^2\,\text{s}^{-2}}, \end{split} \tag{1}$$

where the MLLCL term is set to 1.0 when MLLCL < 1000 m, and set to 0.0 when MLLCL > 2000 m; the MLCIN term is set to 1.0 when MLCIN > $-50\,\mathrm{J\,kg^{-1}}$, and set to 0.0 when MLCIN < $-200\,\mathrm{J\,kg^{-1}}$; the EBWD term is capped at a value of 1.5 for EBWD > 30 m s $^{-1}$, and set to 0.0 when EBWD < 12.5 m s $^{-1}$. The 0–500-m layer used for SRH integration is required to be within the effective inflow layer (or else the parameter is set to 0.0), in order to omit cases that are not likely to be surface based.

Box-and-whisker plots for the five STP500 components and the resulting value of the composite parameter from Eq. (1) for the SFCOA are compared with those from ERA5 for the original U.S. cases (Fig. 2). Qualitatively, the distributions are quite similar for each component, with no notable difference

between thermodynamic and kinematic parameters. As in C19, SRH500, EBWD, and MLLCL (in that order) show the greatest discrimination between significantly tornadic and severe, nontornadic supercells in both datasets. Quantitatively, kinematic variables are more similar between analyses than their thermodynamic counterparts (Table 2). For example, for MLCAPE, the SFCOA has an overall positive difference of means of 86 J kg $^{-1}$ compared to the ERA5, with a correlation of 0.63 and a mean absolute deviation (MAD) of 571 J kg $^{-1}$. The ERA5 struggles the most in high CAPE regimes (>1500 J kg $^{-1}$) compared to the SFCOA, evidenced by lower 90th percentile whiskers and upper quartiles for the

³The terms "difference of means" and "deviation" are preferred to "bias" and "error," respectively, when comparing the two datasets because the latter terms imply a known ground truth, which is not available for these model-based proximity soundings.

TABLE 2. Deviation statistics between the SFCOA and the ERA5 for each component of the effective-layer STP using the 0–500 m AGL SRH (SRH500; m² s⁻²) for all right-moving supercell events. Statistics shown are the difference of means (SFCOA – ERA5), the Pearson correlation coeffecient, and the mean absolute deviation. The STP components are as follows: MLCAPE, MLCIN, MLLCL, EBWD, and SRH500.

	Difference of means		Correlation			MAD			
	Nontornadic	Weakly tornadic	Significantly tornadic	Nontornadic	Weakly tornadic	Significantly tornadic	Nontornadic	Weakly tornadic	Significantly tornadic
MLCAPE	105.5	55.91	101.0	0.5993	0.6632	0.6445	596.5	533.4	585.7
MLCIN	4.996	3.527	2.165	0.4919	0.3779	0.3294	40.52	28.56	30.54
MLLCL	-49.61	7.811	24.17	0.6906	0.6866	0.5789	313.9	255.1	255.5
EBWD	0.8846	0.4086	0.2816	0.6471	0.7216	0.6499	3.965	3.711	3.890
SRH500	8.476	14.59	33.41	0.7677	0.7871	0.7008	45.23	51.22	70.96
STP500	0.0149	0.0852	0.3579	0.4884	0.4883	0.4721	0.6839	0.9928	1.8168

ERA5 in Fig. 2a. Comparatively, the correlation between the reanalyses for MLCIN is worse (0.47); MLCIN was also the most dissimilar in the reanalyses studied by King and Kennedy (2019) and Taszarek et al. (2018), which may be indicative of the struggle for many models to represent capping inversions in severe weather environments (e.g., Nevius and Evans 2018). On the other hand, the correlation between the datasets is more similar for the EBWD and SRH500 (Table 2). For SRH500, the SFCOA has an overall positive difference of means of 12 m² s⁻² compared to the ERA5, with a correlation of 0.80 and a MAD of 49.57 m² s⁻². These deviation statistics slightly degrade when considering deeper layers of SRH (not shown), likely due to cumulative errors while integrating SRH (i.e., errors within the 0–500 m AGL layer are also present in 0–3 km AGL layer).

Collectively, this indicates that the ERA5 agrees more closely with the SFCOA for the wind profile, especially in the lower troposphere, which is similar to results from previous studies comparing shear parameters between reanalyses and observed wind profiles (Allen and Karoly 2014; Gensini et al. 2014; Taszarek et al. 2018). Despite the higher MAD and lower correlations in convective storm thermodynamic environments, the ERA5 is more consistent to the SFCOA compared to its predecessor the ERA-Interim. When King and Kennedy (2019) compared RUC proximity soundings of U.S. supercell events to a host of global reanalyses, the ERA-Interim had negative difference of means in MLCAPE of over 1000 J kg⁻¹, an order of magnitude greater (and opposite sign) than that of the ERA5 shown here (Table 2). The ERA5's increased spatial/temporal resolution and improved data assimilation/model physics appears to result in more faithful representation of the near-storm environment (as in Li et al. 2020; Taszarek et al. 2020a,b).

To further compare the wind profiles between the SFCOA and ERA5, mean hodographs and distributions of the nearground vertical wind shear are constructed. The mean hodographs from the SFCOA (Fig. 3a) are remarkably similar to those in Markowski et al. (2003, see their Fig. 12). Many of the conclusions from that study also apply to the C19 SFCOA dataset, including: similar storm-relative wind speeds through the lower to middle troposphere, significantly larger vertical wind shear and streamwise vorticity in the lowest 1 km for significantly tornadic supercells, and practically indistinguishable shapes of the mean hodographs above 1 km. Compared to the

SFCOA, the ERA5 mean hodographs (Fig. 3b) have similar shapes and orientations, albeit with a slightly less easterly component to the wind direction in the lowest 1 km AGL, especially for the significantly tornadic profile. But, in both analyses, the magnitude of the lower-tropospheric vertical wind shear, especially in the lowest 500 m AGL, is clearly the main discriminatory difference between nontornadic, weakly tornadic, and significantly tornadic wind profiles.

Specifically comparing the distributions of the 0-500 m AGL vertical wind shear (both the direction and magnitude components; Fig. 4) again paints a very similar picture between the two reanalysis datasets. In these rose diagrams, both datasets have lower-tropospheric vertical wind shear primarily oriented toward north, regardless of whether the profile was associated with a nontornadic or significantly tornadic supercell. Across both reanalyses, environments supportive of nontornadic supercells do, however, have a wider distribution in the direction of lower-tropospheric wind shear and regularly have much lower wind shear magnitudes (Fig. 4). The ERA5 does once more show its slight tendency to have more profiles with a 0-500-m wind shear direction oriented toward the north northeast. Overall, the ERA5 does appear to contain a distribution of near-ground wind profiles that is consistent with the SFCOA dataset. Thus, the primary goal of this paper, to capitalize on the ERA5's finer vertical resolution to further investigate the near-ground wind profile, appears justified.4

b. Near-ground storm-relative helicity in supercell environments using the ERA5

SRH has been used as an effective discriminator between tornadic and nontornadic thunderstorms since the concept was

⁴Coarsening the ERA5 soundings to the same isobaric grid in the archived SFCOA profiles results in similar distributions for common convective forecasting variables. This could be taken to mean that the benefits of finer resolution in the ERA5 accrue largely on the "analysis end," where the model's initial guess and the observations themselves retain more finescale structures. In other words, the benefits of the ERA5 profiles are not solely from the vertical grid spacing of the output, although this improved resolution allows for the computation of SRH for shallower layers than otherwise could be with the SFCOA.

United States severe supercell hodographs

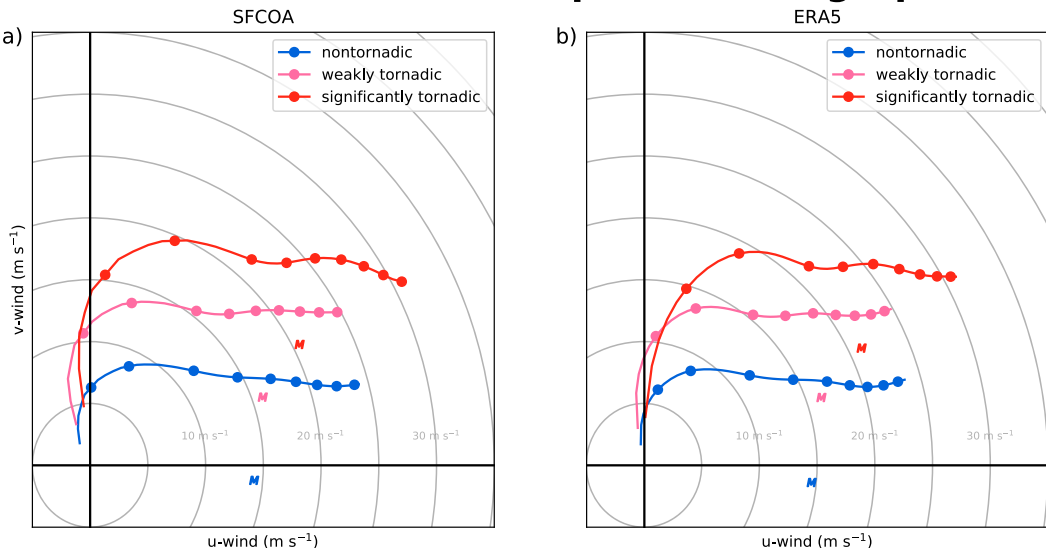


FIG. 3. Mean hodographs of right-moving supercell events in the United States from Coffer et al. (2019), separated by significant tornadoes [(E)F2+; red], weak tornadoes [(E)F0-1; pink], and severe nontornadic supercells (blue) using the (a) SFCOA and (b) ERA5 reanalyses. The mean storm motion (Bunkers et al. 2000) for each profile is indicated with a "M." Each profile was interpolated to a standard height grid, with circle markers indicating heights of 500 m AGL and every kilometer between 1 and 8 km AGL.

first envisioned by Davies-Jones (1984). The calculation of SRH requires a specified layer of winds over which to integrate the dot product of streamwise horizontal vorticity and stormrelative velocity. Initially, this was commonly performed over the lowest 3 km of the atmosphere, representing an approximate depth of inflow into a mature supercell. However, since the early- to mid-2000s, a consensus has emerged that the characteristics of the wind profile in the lower troposphere (~0-1 km AGL) are the most determinative to the eventual likelihood of tornadogenesis (e.g., Markowski et al. 1998, 2003; Rasmussen and Blanchard 1998; Rasmussen 2003; Monteverdi et al. 2003; Thompson et al. 2003; Craven et al. 2004). Of all the components of the STP500 in Eq. (1), C19 found SRH in the 0-500 m AGL layer to be the most skillful at distinguishing between nontornadic and significantly tornadic supercells. Parcels with high magnitudes of streamwise horizontal vorticity near the surface are the most likely to contribute to intense low-level mesocyclones via tilting. Coffer and Parker (2017) showed that the environmental parcels that made up the lowlevel mesocyclones (~1 km AGL), in both a nontornadic and tornadic supercell, originated exclusively from below 300 m, with the median parcel height starting near 180 m AGL.

In light of this, perhaps the most skillful layer of SRH is even shallower than the 0–500 m AGL layer. In this section, we test that hypothesis using the ERA5 reanalysis. SRH is calculated over a multitude of depths (50, 100, 150, 200, 250, 300, 400, 500, 750, 1000, 2000, and 3000 m), using the original Bunkers storm motion estimate for right-moving supercells (Bunkers et al. 2000) with a 0–6-km height-based mean wind (Bunkers et al. 2014). Forecast skill for each depth is evaluated using the TSS as a measure of discrimination between nontornadic and

significantly tornadic supercells, with the optimal threshold being the highest value of TSS for each forecast parameter.

SRH is a quite skillful parameter, almost regardless of the chosen depth of integration. However, progressively shallower depths do generally result in increased discrimination when comparing significantly tornadic supercells to nontornadic supercells (Fig. 5). Each subsequent, shallower layer tends to have higher forecast skill than deeper layers; however, the gains in TSS saturate in the lowest few hundred meters (Table 3, Fig. 6). Nationwide across the United States, the biggest jump in forecast skill occurs when SRH calculations are made over a depth decreasing from the 0-3 km AGL layer to the 0-1 km AGL layer (Table 3, Fig. 6). Further focusing to the 0-500 m AGL layer provides yet another increase in forecast skill (TSS_{SRH500} = 0.51), which led Coffer et al. (2019) to include this layer in an updated version of the STP. A final increase in forecast skill is present when integrating only over the lowest couple hundred meters, with the 0-100 m AGL (SRH100) layer having the highest TSS of any SRH layer tested herein ($TSS_{SRH100} = 0.53$). Admittedly, these additional increases in TSS are small; however, they do represent meaningful improvements in forecast skill. Compared to a depth of $500\,\text{m}$, the increase in TSS_{SRH100} corresponds to 8.2% more correctly identified events (i.e., hits and correct nulls) and a 19.6% decrease in incorrectly identified events (i.e., misses and false alarms). Other metrics besides TSS show similar improvements in forecast skill with shallower layers. The best combinations of POD, FAR, and CSI occur for SRH in layers shallower than 500 m (Fig. 7).

As might be expected, there is regional variance in the forecast skill of differing layers of SRH. Using the same

0 - 500 m wind shear

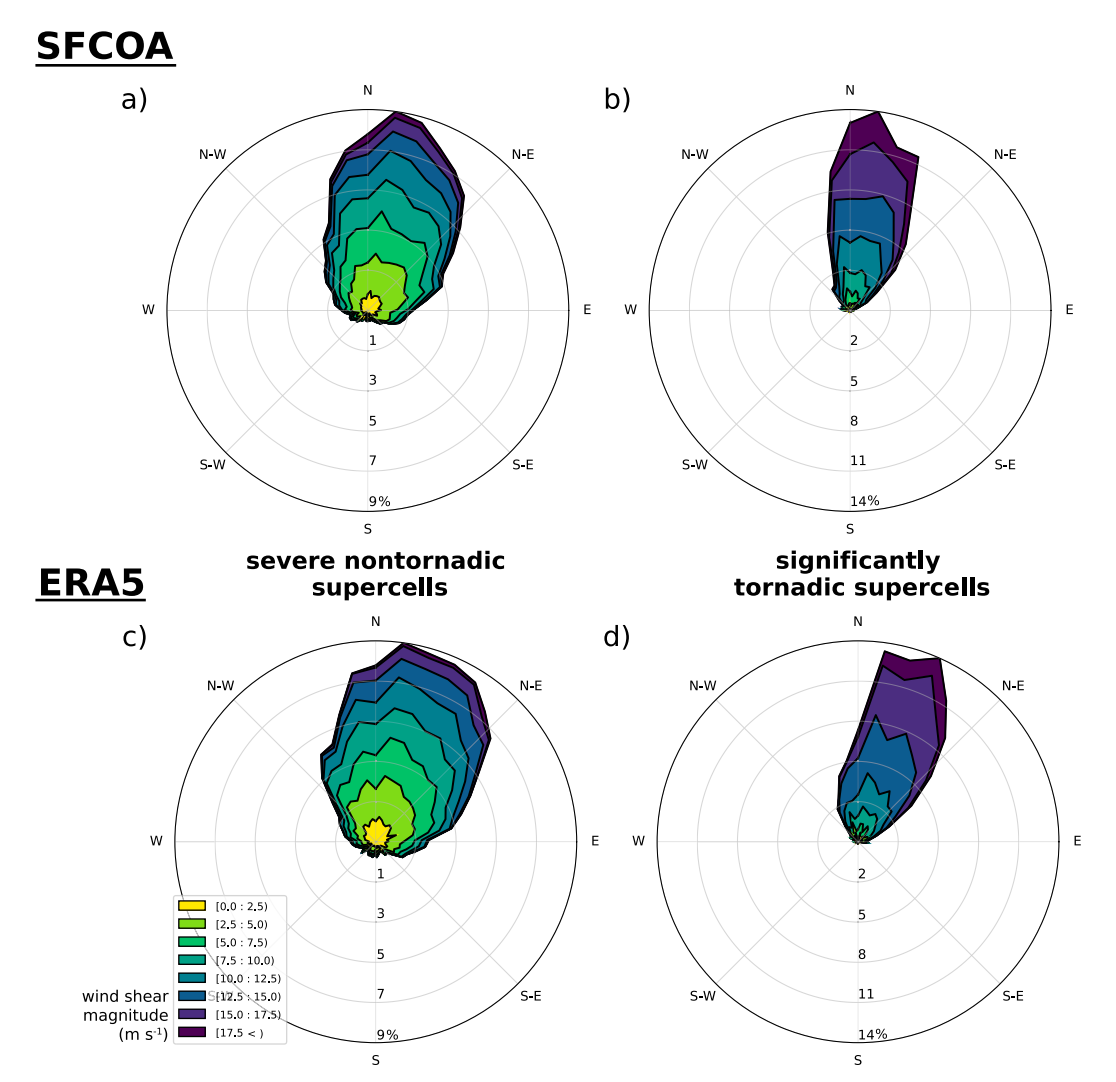


FIG. 4. Wind rose diagram showing 0–500-m wind shear direction (S, SE, E, etc.) and wind shear magnitude (shaded) for (a),(c) severe nontornadic supercells and (b),(d) significantly tornadic supercells in both the (top) SFCOA and (bottom) ERA5. Wind direction is separated into 45 bins. Percentages of each dataset are labeled accordingly along the southern axis.

geographic regions as C19 (see their Fig. 1a), SRH100 is most skillful in Northeast, South Atlantic, Upper Mississippi Valley, and the western United States (although the sample size of significantly tornadic supercells is particularly small west of the Rocky Mountains). The forecast skill of SRH100 is slightly lower than the national average in the both the northern and southern Great Plains (TSS_{SRH100} = 0.46, 0.50), and quite a bit lower in the Lower Mississippi Valley (TSS_{SRH100} = 0.39). Most of the regional SRH100 trends in the ERA5 dataset track well with the SRH500 results found in the SFCOA dataset by C19. The main outlier is the forecast skill of near-ground SRH in the southeast United States (which includes the Lower Mississippi Valley and South Atlantic). While SRH is by far the most skillful parameter tested herein, including in the

Southeast, TSS_{SRH500} in this region is considerably lower in the ERA5 compared to the SFCOA (Fig. 6; ERA5: dashed cyan line versus SFCOA: cyan dots). Using the ERA5, TSS for SRH in the Southeast throughout the lowest 3 km AGL is essentially a uniform profile (Fig. 6). The reason for the lower forecast skill in the ERA5 is related to the 0–500-m shear vector for significantly tornadic supercells being on average more veered in the ERA5 dataset compared to the SFCOA (Figs. 3 and 4), as mentioned in section 3a. This is notably a bigger difference in Southeast composite hodographs (not shown). The veering of the shear vector in the lowest few hundred meters results in less area swept out between the hodograph and the storm motion, thus reducing the near-ground SRH. Because this is most prevalent in the significantly tornadic

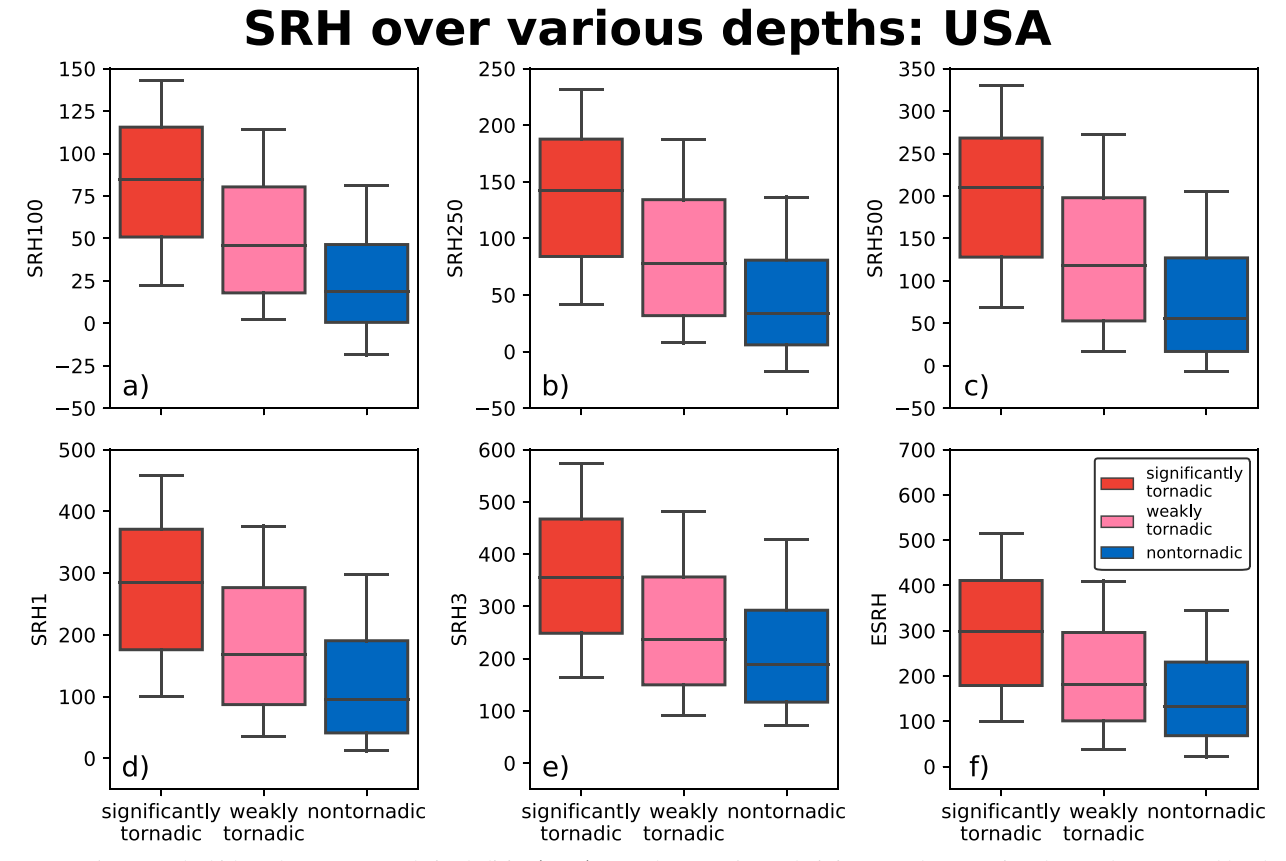


FIG. 5. Box-and-whisker plots of storm-relative helicity (SRH) from the ERA5 reanalysis integrated over various layers above ground level (AGL): (a) 0-100 m (SRH100), (b) 0-250 m (SRH250), (c) 0-500 m (SRH500), (d) 0-1 km (SRH1), 0-3 km (SRH3), and the effective inflow layer (ESRH), separated by significant tornadoes [(E)F2+; red, n=1612], weak tornadoes [(E)F0-1; pink, n=7743], and severe nontornadic supercells (blue, n=10839). The whiskers extend upward to the 90th and downward to the 10th percentiles. Outliers are excluded for clarity.

subset of supercells, the overall forecast skill of the SRH is therefore reduced. In fact, while the correlation between the ERA5 and SFCOA is highest with the near-ground wind profile (as shown in section 3a), each of the metrics are

worse for significantly tornadic supercells in the Southeast compared to the whole dataset (difference of means: 12 versus $41 \text{ m}^2 \text{ s}^{-2}$, correlation: 0.80 versus 0.68, MAD: 49.57 versus $74.95 \text{ m}^2 \text{ s}^{-2}$).

TABLE 3. Best TSS and optimal threshold of SRH (m² s -2) from the ERA5 reanalysis integrated over various layers AGL for discriminating between significant tornadoes (EF2+) and severe nontornadic events in the United States and Europe. TSS is calculated at 1000 evenly spaced thresholds between the 1st and 99th percentile for each layer.

	U	nited States	Europe		
	Max TSS	Optimal threshold	Max TSS	Optimal threshold	
SRH50	0.5271	33.06	0.4038	9.958	
SRH100	0.5304	48.71	0.4156	10.74	
SRH150	0.5247	56.94	0.4223	14.76	
SRH200	0.5240	55.96	0.4285	19.08	
SRH250	0.5226	63.42	0.4308	22.09	
SRH300	0.5191	78.01	0.4254	30.36	
SRH400	0.5136	95.63	0.4120	33.65	
SRH500	0.5080	104.7	0.3999	44.63	
SRH750	0.4886	117.3	0.3575	69.60	
SRH1	0.4786	148.6	0.3278	89.36	
SRH2	0.4356	258.1	0.2369	101.8	
SRH3	0.4162	274.0	0.1834	133.9	
ESRH	0.3925	263.8	0.1255	107.5	

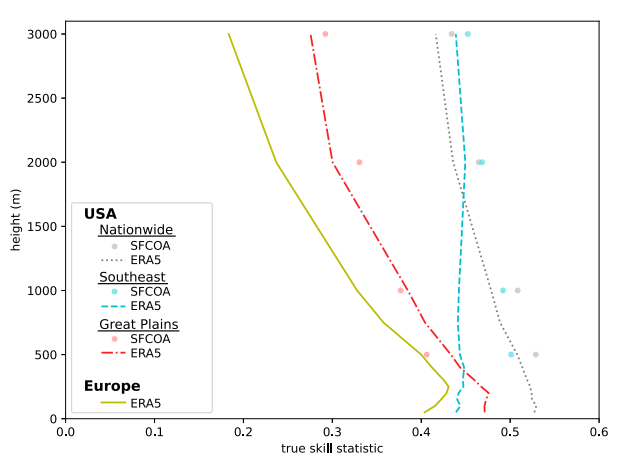


FIG. 6. True skill statistic (TSS) at the optimal threshold for various depths of SRH integrated from 50 to 3000 m AGL for discriminating between significant tornadoes (EF2+) and severe nontornadic supercells from the ERA5 reanalysis. Shown are the distributions across the entire United States (gray dotted line; Table 3), the Southeast United States (cyan dashed line), the plains region of the United States (red dash–dot line), and in Europe (olive solid line). Regions from the United States are shown in Coffer et al. (2019, their Fig. 1a). TSS of SRH integrated at 500, 1000, 2000, and 3000 m AGL in SFCOA are shown as dots for the USA regions using the same colors as indicated in the legend. TSS is calculated at 1000 evenly spaced thresholds between the 1st and 99th percentile of the entire ERA5 sounding dataset for each layer.

An obvious question here is whether using wind profiles in the lowest few hundred meters of the atmosphere from modelbased reanalyses is even appropriate, given errors in the analyses are usually highest in the PBL (Coniglio et al. 2013; Clark et al. 2015) and oftentimes this analysis is focused on what might be considered the surface layer (i.e., the lowest 10% of the PBL; Stull 1988). How well either the SFCOA or the ERA5 represent the near-ground wind profile ostensibly might not matter for operational forecasters since these analyses are the best routinely available estimates of the current state of the atmosphere in lieu of targeted near-storm soundings. Consequently, the presence of forecast skill for analyzed nearground SRH is useful. Further improvements in the representation of the near-ground wind profile in reanalysis datasets might further confirm (or deny) the forecast value of surface layer SRH, or even highlight other components of the wind profile that are not skillful in the current datasets, such as crosswise horizontal vorticity.

Departing from previous studies (including C19 and the analysis herein), Coniglio and Parker (2020) found that, when compiling hundreds of observed proximity soundings obtained from various field programs, deeper layers of SRH were more statistically different between nontornadic, tornadic, and significantly tornadic supercells, due to larger storm-relative winds in the significantly tornadic cases. The larger storm-relative winds were the result of the combination of ground-relative winds that were twice as strong on average and more deviant rightward storm motions compared to nontornadic soundings (Coniglio and Parker 2020). Because the observed

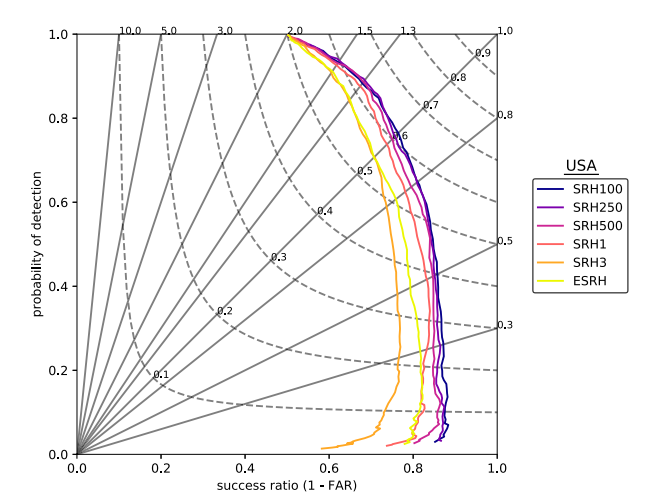


FIG. 7. Performance diagram (Roebber 2009) summarizing the success ratio [1 – FAR (false alarm ratio)], probability of detection, bias, and critical success index at 1000 evenly spaced thresholds between the 1st and 99th percentile for each SRH layer from Fig. 5. Shown is the discrimination between significant tornadoes (EF2+) and severe nontornadic supercells from the ERA5 reanalysis. Solid lines represent bias scores with labels on the outward extension of the line, while labeled dashed contours are the critical success index (CSI), which has similar trends to the TSS.

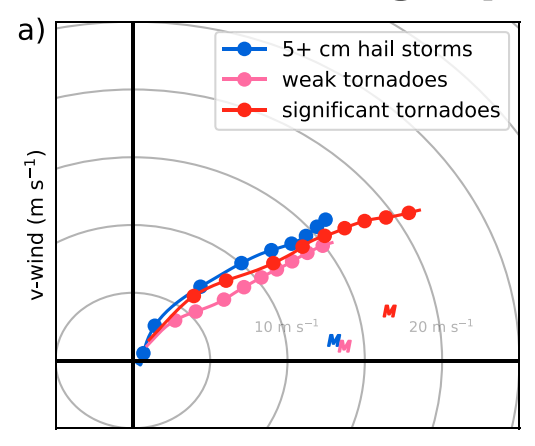
storm motion is not available for the 20194 supercell cases from the SPC storm mode database, it is impossible to know whether more deviant storm motions would cause deeper layers of SRH to be more skillful. While the Bunkers storm motion estimate (Bunkers et al. 2000) is currently the best available method of diagnosing off-hodograph propagation of supercells, it does have known biases, especially for significantly tornadic supercells with large 0–3 km AGL SRH (Bunkers 2018). However, as an operational consideration, the Bunkers motion is the most uniformly available for SRH calculations (and the only estimate prior to storm formation). As in C19, we find that in real-time operational settings, shallower layers of SRH provide the greatest discrimination between nontornadic and significantly tornadic supercells.

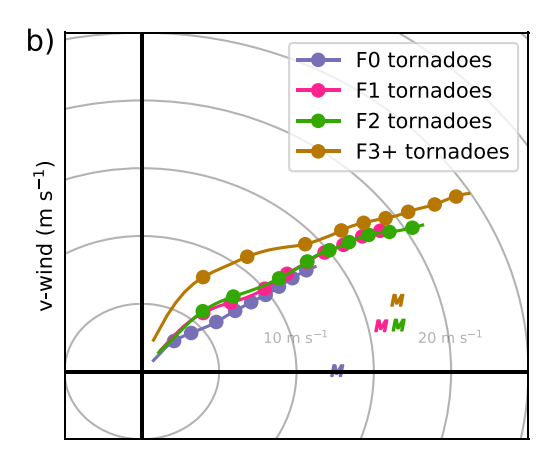
4. Europe

a. Near-ground wind profiles

Given the success of using SRH in layers very near the ground in discriminating between nontornadic and significantly tornadic supercells in the United States, we next investigate whether the same forecasting principles can be applied to European severe thunderstorm forecasting. It is perhaps unreasonable to expect environmental proxies used in the United States to be easily transferable from continent to continent, especially as the value of these proxies are regionally and seasonally dependent even within the United States. Over Europe, Púčik et al. (2015) found that shallower layers of SRH had more "overlap between intensity categories for all events" than deeper layers (i.e., shallow layers had less forecast skill); however, they speculated that high spatial and temporal

European severe weather hodographs





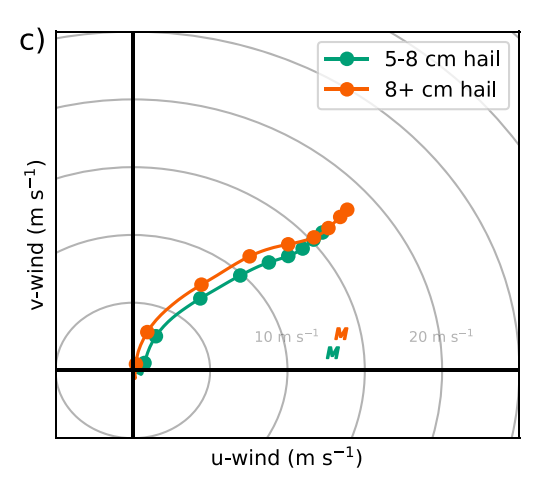


FIG. 8. Mean hodographs of significantly severe hail and tornado reports from the ESWD during the years 1979–2019 using the ERA5 reanalysis. Each profile was interpolated to a standard height grid, with circle markers indicating heights of 500 m AGL and every kilometer between 1 and 8 km AGL. (a) Separated into

variability of SRH (especially near the ground) may explain this result in their study. Taszarek et al. (2017) also found that that 0–3 km AGL vertical wind shear has more skill in discriminating among weak and significant tornadoes, more so than 0–1 km AGL vertical wind shear or SRH. The spatiotemporal advantages of the ERA5 compared to balloon-borne radiosonde observations should yield more faithful insights into environmental differences between nontornadic and significantly tornadic thunderstorms than was possible in previous studies.

Compared to the mean hodographs from the United States, those associated with European severe weather events on average have much straighter hodographs, especially in the lowest couple kilometers of the atmosphere (cf. Figs. 3b and 8a). The straight lower-tropospheric hodograph in Europe is possibly due to the lack of a favorable orography/coastline orientation to support strong low-level jet formation compared to the United States. One implication of these straighter hodographs is that storms will initially have weaker updrafts with less correlated vorticity (Weisman and Rotunno 2000). With a storm motion that initially resides along the mean wind vector, straight hodograph environments rely on updraft propagation off the hodograph via pressure perturbations from the dynamically forced, rotating updraft in order to access potential SRH in the environment. The European tornadic hodographs more closely resemble those of multicellular, hail storms in North American (Chisholm and Renick 1972) than the tornadic supercells profiles in Fig. 3. Thunderstorms that produce large hail in European environments have sufficient deep-layer shear (i.e., 0-6 km AGL) to support supercell formation, but most of that shear is concentrated in the 1-3 km AGL layer rather than in the lower troposphere. Recent modeling on U.S. hailstorms has shown that increased shear in this layer is favorable for larger hail growth (Dennis and Kumjian 2017; Kumjian and Lombardo 2020).

The most striking difference between the hodographs of European nontornadic and tornadic severe thunderstorms is the magnitude of the lower-tropospheric winds, specifically below 500 m AGL (i.e., the first dot in Fig. 8a). There is almost no flow below 500 m on average in the severe nontornadic thunderstorms and what little structure is present in the hodograph represents primarily *anti-streamwise* horizontal vorticity. This is also reflected in the distributions of near-ground SRH in the nontornadic environments, as over half the cases had zero or negative SRH in the lowest 500 m AGL (Fig. 9c). The tornadic environments, especially for significantly tornadic thunderstorms, have much larger near-ground vertical wind shear. The average 0–500 m AGL wind shear magnitude increases from 0.88 m s⁻¹ in the nontornadic environments to 6.72 m s⁻¹ for

←

significant tornadoes (F2+; red), weak tornadoes (F0-1; pink), and severe nontornadic storms (blue). (b) Separated into F0 tornadoes (purple), F1 tornadoes (magenta), F2 tornadoes (green), and F3+tornadoes (brown). (c) Separated into 5–8-cm hail (green) and >8-cm hail (orange). The mean storm motion (Bunkers et al. 2000) for each profile is indicated with a "M."

SRH over various depths: Europe

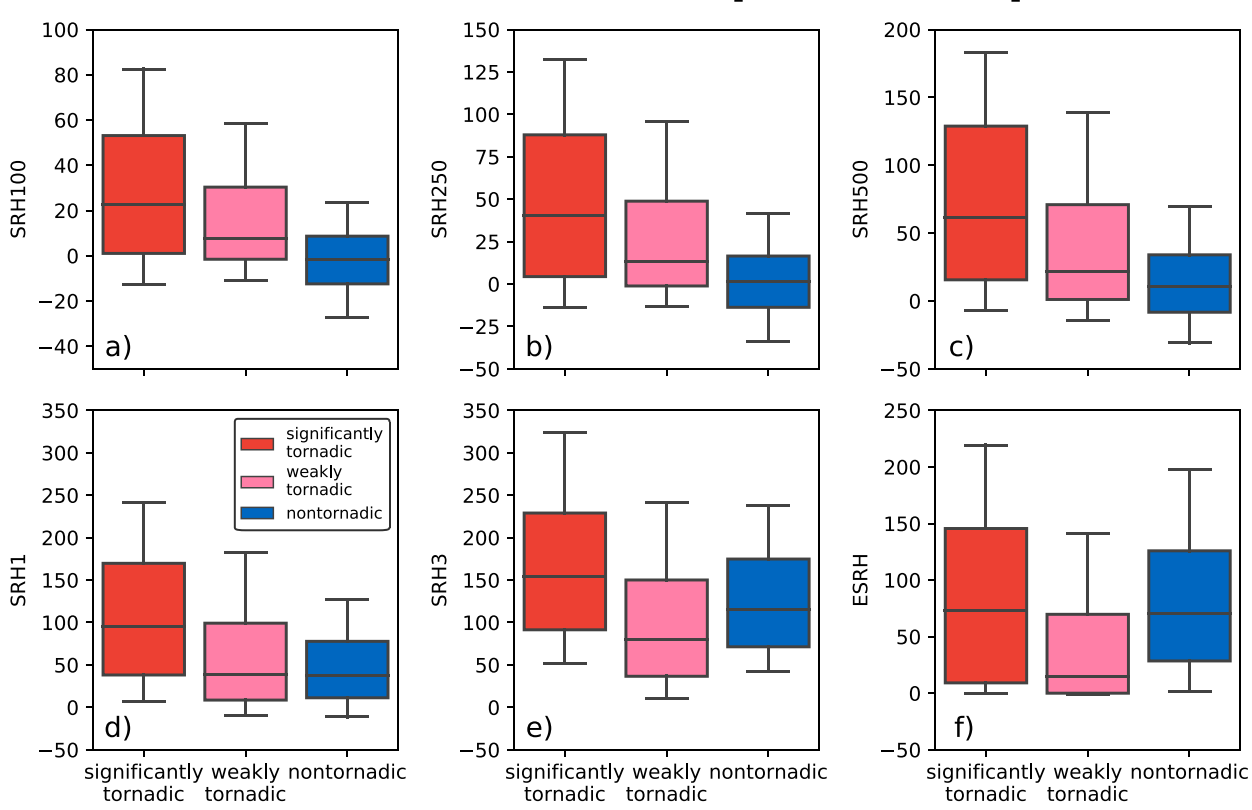


FIG. 9. Box-and-whisker plots of SRH from the ERA5 reanalysis integrated over various layers AGL: (a) $0-100 \,\mathrm{m}$ (SRH100), (b) $0-250 \,\mathrm{m}$ (SRH250), (c) $0-500 \,\mathrm{m}$ (SRH500), (d) $0-1 \,\mathrm{km}$ (SRH1), $0-3 \,\mathrm{km}$ (SRH3), and the effective inflow layer (ESRH), separated by significant tornadoes (F2+; red, n=479), weak tornadoes (F0-1; pink, n=3060), and severe nontornadic storms (blue, n=1247) from the ESWD during the years 1979–2019. The whiskers extend upward to the 90th and downward to the 10th percentiles. Outliers are excluded for clarity.

significantly tornadic events. Environments that supported significantly tornadic thunderstorms also have much faster wind speeds between 3 and 8 km AGL, which is perhaps indicative of more amplified synoptic environments.

Separating the European composite hodographs into the more specific subclasses reveals a few more interesting details (Figs. 8b,c). Thunderstorms that produce large (e.g., 5–8 cm) versus giant hail (e.g., >8 cm) have similar overall shapes; however, environments supportive of giant hail tend to have more curvature in the hodograph in the lower troposphere (and thus more SRH), higher shear in the 1-3 km AGL layer, and faster winds in the upper troposphere. Weaker F0 tornadoes on average have less shear throughout the lower troposphere and weaker winds aloft, similar to the findings of Taszarek et al. (2017, 2020b). The composite hodographs for tornadoes rated F1 and F2 are surprisingly similar, with F2 tornadoes having slightly more shear above 1 km AGL. Tornadoes that cause severe and devastating damage (i.e., ratings of F3 and F4) notably have more curvature in the hodograph, especially in the lowest 500 m (leading to more SRH). The average wind speed at 2 km AGL for F3+ tornadoes is faster than the entire 8 km AGL wind profile for F0 tornadoes.

In U.S. supercell environments, SRH is skillful at discriminating between significantly tornadic supercells and

nontornadic supercells over almost any depth of integration; however, the same cannot be said of European severe weather environments. Even though the overall forecast skill of SRH is lower in Europe than the United States (Table 3), the benefits of using shallower layers is even more consequential (Fig. 6, cf. Figs. 7 and 10). The near-ground wind profile is markedly different between significantly tornadic and nontornadic thunderstorm environments in Europe, resulting in increased forecast skill (albeit with lower overall magnitudes of SRH than in the United States). Going from the 0-3 km AGL layer to the 0-250 m layer, the TSS increases from 0.18 to 0.43 (Table 3). Nearly 50% of the nontornadic subset of thunderstorms in Europe has negative SRH in the lowest 500 m AGL (Fig. 9c). Minimal or negative SRH is even more prevalent in shallower layers, such as 100 or 250 m AGL (Figs. 9a,b).⁵ In contrast, deeper layers of SRH in Europe have considerably

⁵The nontornadic thunderstorm environments still possess plenty of surface-based CAPE and minimal surface-based CIN (not shown), which suggests the weak flow at the surface is not indicative of the mesoscale regime being postfrontal or elevated for these cases.

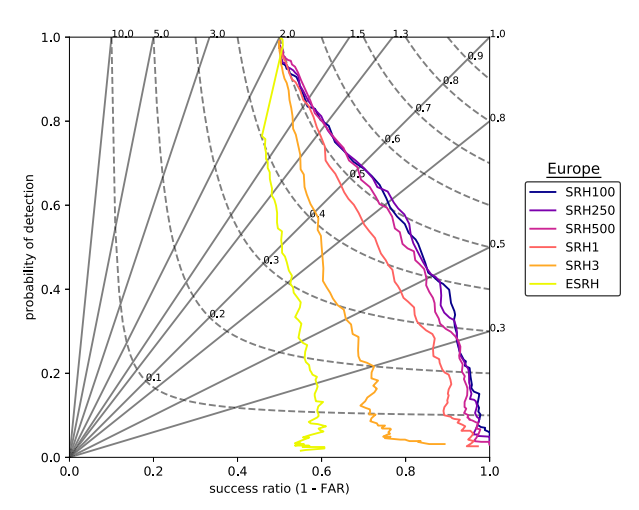


FIG. 10. Performance diagram (Roebber 2009) summarizing the success ratio [1 – FAR (false alarm ratio)], probability of detection, bias, and critical success index at 1000 evenly spaced thresholds between the 1st and 99th percentile for each SRH layer from Fig. 9. Shown is the discrimination between significant tornadoes (EF2+) and severe nontornadic storms from the ERA5 reanalysis. Solid lines represent bias scores with labels on the outward extension of the line, while labeled dashed contours are the CSI, which has similar trends to the TSS.

more overlap between nontornadic and significantly tornadic thunderstorms (Figs. 9c,d). Several indices, such as MLLCL and MLCIN, have as much forecast skill as SRH1 and considerably more forecast skill than SRH3 (Tables 3 and 4). The

effective-layer SRH is even worse than SRH3 (Figs. 9c,d), exhibiting essentially zero forecast skill (Table 3; for reasons that will be discussed below).

b. Significant tornado parameter for European severe weather environments

Although the main focus of this paper is on the near-ground wind profile, it is worth exploring the utility of the STP using SRH in the 0-500 m AGL layer in European severe weather environments. The individual components of STP have varying degrees of utility across Europe, just as they do in the United States. In contrast to the United States, however, the combination of parameters in Eq. (1) do not result appreciable forecast skill between significantly tornadic and severe, nontornadic thunderstorms (Table 4). The median STP500 for both significant tornadoes and nontornadic thunderstorms is essentially zero (Fig. 11), and the overall TSS_{STP500} is a meager 0.17. Despite, the low forecast skill of STP500, it is a considerable improvement over the supercell composite parameter (SCP) and the effective-layer version of the STP (Table 4). Still, the lack of forecast skill in the STP500 in European severe weather environments is the result of physical differences between European and U.S. severe weather environments, as well as nonphysical choices in the design of the parameter (i.e., optimizing it for the U.S. dataset it was intended for).

First, MLCAPE has substantial negative forecast skill at distinguishing between significantly tornadic and severe, nontornadic thunderstorms (TSS_{MLCAPE} = -0.346; i.e., MLCAPE is higher for severe hailstorms than significant tornado events). Larger CAPE is almost certainly not detrimental to the

TABLE 4. Best TSS and optimal threshold for given forecasting parameters from the ERA5 reanalysis for discriminating between significant tornadoes (EF2+) and severe nontornadic events in the United States and Europe. TSS is calculated at 1000 evenly spaced thresholds between the 1st and 99th percentile for each variable. The forecasting parameters are as follows: surface-based (SB) and mixed-layer (ML; lowest 100 hPa) convective available potential energy (SBCAPE/MLCAPE), convective inhibition (SBCIN/MLCIN), and height of the lifted condensation level (SBLCL/MLLCL), 0–3 km AGL MLCAPE (3CAPE), vertical wind shear magnitude in the layers of 0–500 m AGL (500SHR), 0–1 km AGL (1SHR), 0–3 km AGL (3SHR), and 0–6 km AGL (6SHR), the effective bulk wind difference (EBWD), the critical angle (CA), as well as the supercell composite parameter (SCP) and two variants of the significant tornado parameter, the effective layer (STP) and the STP with 0–500 m AGL SRH (STP500).

	U	nited States	Europe		
	Max TSS	Optimal threshold	Max TSS	Optimal threshold	
SBCAPE	0.028	42.47	0.0	_	
SBCIN	0.1660	142.6	0.1339	42.58	
SBLCL	0.3169	404.5	0.2894	454.4	
MLCAPE	0.0383	152.5	0.0	_	
MLCIN	0.169	14.20	0.2955	21.60	
MLLCL	0.3342	955.2	0.3041	901.8	
3CAPE	0.1515	61.57	0.1049	17.45	
500SHR	0.5220	9.405	0.4111	4.917	
1SHR	0.5159	11.789	0.3974	6.469	
3SHR	0.4396	18.56	0.2384	13.64	
6SHR	0.3399	24.93	0.1820	20.96	
EBWD	0.3393	24.68	0.0821	16.17	
CA	0.0321	26.01	0.0034	9.841	
SCP	0.3105	5.056	0.0131	0.0	
STP	0.3780	0.9076	0.0121	0.0	
STP500	0.4372	0.7201	0.1701	0.1229	

STP500 components: Europe

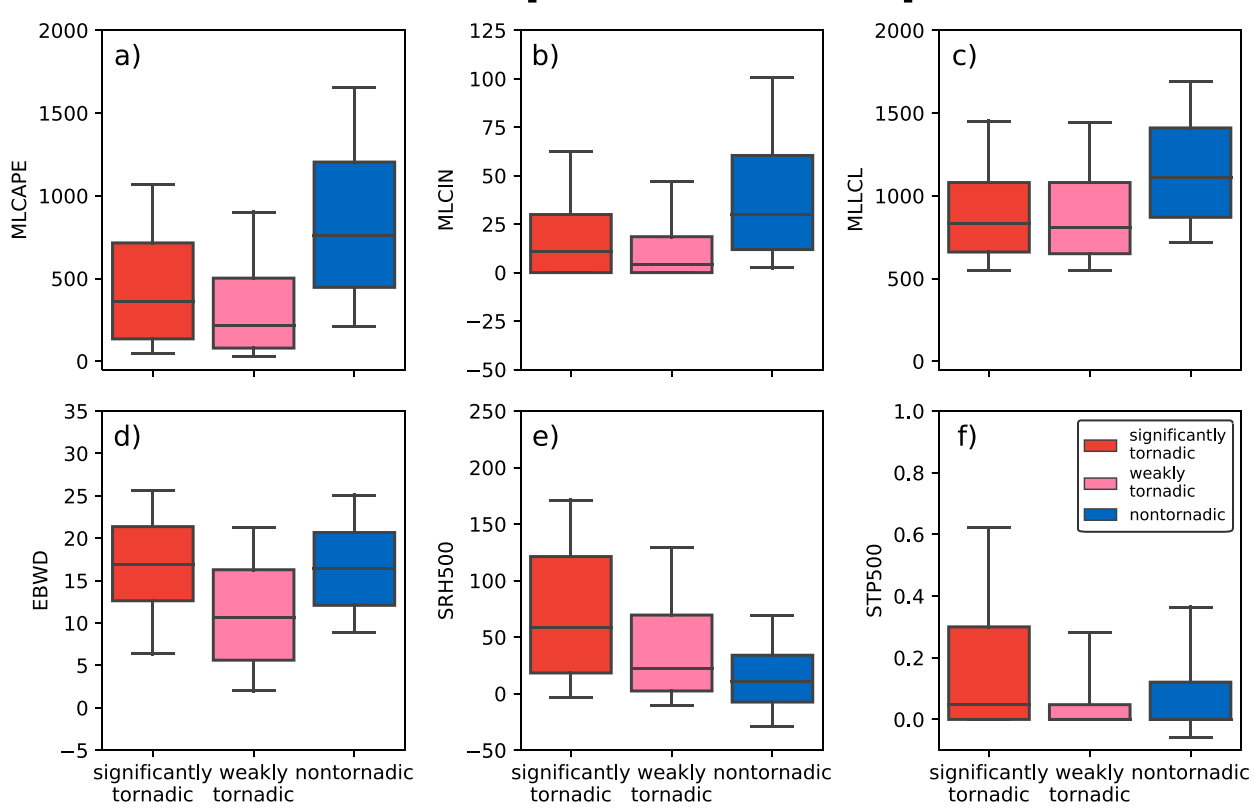


FIG. 11. Box-and-whisker plots of each component of the effective-layer STP using the 0–500 m AGL SRH (SRH500; m² s⁻²) from the ERA5 reanalysis for all right-moving supercell events, separated by significant tornadoes (F2+; red, n = 479), weak tornadoes (F0–1; pink, n = 3060), and severe nontornadic storms (blue, n = 1247) from the ESWD during the years 1979–2019. The components are as follows: (a) MLCAPE, (b) MLCIN, (c) MLLCL, (d) EBWD, and (e) SRH500. (f) The resulting distributions of the STP500 composite parameter. The whiskers extend upward to the 90th and downward to the 10th percentiles. Outliers are excluded for clarity.

tornadogenesis process (in contrast to MLCIN and MLLCL). Instead, the negative skill found for CAPE in Europe is likely due to the how the ESWD dataset was filtered to include the most probable supercell events. The filtered ESWD reports used herein do not represent a comprehensive nontornadic thunderstorm sample (absent storm mode information, we used large hail as a simple proxy). Thunderstorms that produce hailstones greater than 5 cm are simply more likely to have higher values of CAPE. In contrast, a large number of significant tornadoes in Europe do appear to occur in low CAPE environments (i.e., MLCAPE $< 500 \,\mathrm{J\,kg^{-1}}$, Fig. 11). Previous research does suggest that the near-ground wind profile is especially important in generating low-level updrafts capable of tornadogenesis with such low CAPE environments (Sherburn and Parker 2014, 2019; Sherburn et al. 2016; Wade and Parker 2020, manuscript submitted to Mon. Wea. Rev.).

Another component of the STP500 calculation with negligible forecast skill is the cutoff applied to the deep-layer vertical wind shear term. The entire parameter is set to zero when the EBWD is $<12.5\,\mathrm{m\,s^{-1}}$. This condition works well for U.S. supercell events due to their typically higher magnitudes compared to European events (cf. Figs. 2d and 11d). In the

United States, almost the entire dataset has an EBWD $> 12.5 \,\mathrm{m\,s^{-1}}$, while in Europe, much of the dataset is below this threshold. This results in STP500 being set to zero for a considerable fraction of the cases in Europe (and may be indicative of storm mode differences).

The last condition of the STP500 that negatively affects its skill in Europe is the use of the effective storm inflow layer and effective storm depth calculations. As noted by Thompson et al. (2007), the effective storm inflow layer can be missing from a sounding due to insufficient buoyancy, excessive convective inhibition, and/or the effective inflow "layer" is a single level in the sounding. Because of the high percentage of soundings with MLCAPE $< 100 \,\mathrm{J\,kg^{-1}}$ (Fig. 11a), the effective inflow layer is often undefined and thus the ESRH for these cases is zero. This helps explain the lack of forecast skill for ESRH compared to fixed-layer calculations of SRH (Fig. 9, Table 4). While STP500 does not use ESRH directly, the effective inflow layer is implicitly used in SRH500 component of Eq. (1) because the 0-500 m AGL layer is required to be within the effective inflow layer. Therefore, if the effective inflow layer is undefined or very shallow in low-CAPE environments, the SRH500 component of the STP500 is set to zero (which

makes the whole parameter zero). This results in the non-tornadic subset having higher ESRH values on average (due to more MLCAPE and deeper effective inflow layers), even though tornadic environments have more lower-tropospheric vertical wind shear.

In summary, the combination of MLCAPE, EBWD, and SRH500 result in a STP that has virtually no value in the European severe weather environments investigated herein. Similarly poor forecast skill of STP across Europe has been also noted by Kaltenböck et al. (2009), Rodríguez and Bech (2018), and Taszarek et al. (2020b). Climatologically, European severe thunderstorm environments almost never reach the kinematic/thermodynamic parameter space as severe thunderstorms in United States due to much lower magnitudes of SRH, CAPE, and deep-layer shear (Taszarek et al. 2020a,b). While modifying the STP for European environments is beyond the scope of this study, preliminary results suggest using fixed layer depths for deep-layer shear (i.e., 0-6 km or 0-3 km AGL vertical wind shear), as well as 0-3-km CAPE (3CAPE) can improve the skill of an ingredients-based forecast parameter (Table 4). Future work could look at a "European calibrated" STP-like parameter, perhaps in a similar manner to the high-shear low-CAPE parameter by Sherburn and Parker (2014), as well as seasonal, diurnal, and regional trends trends of STP performance in Europe. Additionally, integrating radar data (e.g., the OPERA pan-European radar dataset; Huuskonen et al. 2014; Saltikoff et al. 2019) with these reports may allow construction of a database of convective modes (like in the United States). Regardless, for the tornadic and nontornadic report investigated herein, the forecast utility of near-ground SRH for European tornado forecasts appears clear when using the ERA5.

5. Conclusions

This study was motivated by the question of whether shallower layers of SRH integration leads to more forecast skill between significantly tornadic and nontornadic thunderstorms using a newly available reanalysis dataset. Recent studies have suggested that air parcels that originate from very close to the ground, when ingested into the low-level updraft/mesocyclone, exhibit significant control over the organization, intensity, and steadiness of the lifting and stretching required for tornadogenesis to occur. Using the ERA5 reanalysis, proximity soundings from both the United States and Europe show the following most important results:

- The ERA5 represents severe weather environments in the United States similarly to the traditionally used SFCOA, especially the near-ground wind profile. Correlations and deviations between the two reanalysis datasets suggest that the ERA5 is much more similar to the SFCOA than other global reanalysis datasets.
- 2) Progressively shallower layers of SRH have increased forecast skill in discriminating between significant tornadoes and severe, nontornadic supercells in the United States. The 0-100 m AGL layer had the highest forecast skill of any SRH layer tested, however, gains in forecast skill are more modest beyond the 0-500 m AGL layer.

3) In European severe weather environments, the near-ground wind profile is by far the most discriminatory feature of profiles distinguishing significant tornadic events from severe hailstorms. In terms of forecast skill, there is even more benefits in using shallower layers of SRH in Europe compared to the United States. Nontornadic environments often have minimal vertical wind shear near the ground, with many exhibiting antistreamwise horizontal vorticity in the lowest few hundred meters. In contrast, significantly tornadic thunderstorms exhibit much larger lower-tropospheric vertical wind shear and thus near-ground SRH. Near-ground SRH alone is more skillful than the STP (given thunderstorm development). STP itself was much less skillful in Europe than in the United States.

Overall, near-ground SRH is a highly skillful parameter, whether integrated over a 500-m layer or a layer as shallow as 100 m. Either way, it represents a meaningful increase in forecast skill compared to much deeper layers currently used operationally. While C19 recommended including SRH500 into the STP instead of ESRH, using an even shallow layer, such as SRH100, results in just as much of increase in forecast skill (not shown), mostly due to the decrease in the number of incorrectly predicted events. Therefore, a further increase in the operational utility of the STP is possible assuming the data source has sufficient vertical resolution near the ground (and a reliable representation of the PBL). Regardless, as discussed by C19, while STP clearly helps forecasters identify the general area of tornadic thunderstorms, once convection has been initiated and severe thunderstorms seem likely, additional skill in forecasting significant tornadoes can then be gained by looking more specifically at areas of maximized near-ground SRH (i.e., SRH100).

The real-time operational use of SRH from the shallow layers recommended in this work will necessarily require more frequent observations of the near-ground vertical wind profile than what is currently available. The use of unmanned aircraft systems to collect routine in situ vertical profiles within the atmospheric boundary layers appears to be a promising way to achieve this high spatial and temporal sampling of near-storm environments in the future (Chilson et al. 2019; Bell et al. 2020).

Ultimately, further improvements in discriminating between nontornadic and significantly tornadic thunderstorm events may require a breakthrough in our understanding of environmental controls on tornado formation. Essentially, the same five variables (CAPE, CIN, LCL, deep-layer shear, and lowertropospheric SRH) have been staples of every tornadic severe weather forecast for almost 20 years. Given that tornado warning lead time has stalled as of late (Brooks and Correia 2018), the utility of these five variables to distinguish nontornadic from tornadic events with lead times on the order of an hour (or less) may be at its limit (Coffer et al. 2017; Flournoy et al. 2020; Markowski 2020). Future work using deep learning (LeCun et al. 2015; McGovern et al. 2017) of environments associated with various modes of supercell convection may be able to provide insights into novel features associated with environments supportive of nontornadic, weakly tornadic, and significantly tornadic supercell thunderstorms, without any

preconceived notions of what ingredients are most important. Furthermore, incorporating a three-dimensional picture of these environments could yield more predictive information than a single point vertical profile can provide (e.g., surface boundary orientation, shape of the buoyancy profile, upperlevel forcing for ascent, etc.). Nevertheless, the results of this study have shown that advances in our analyses of nearground wind profiles can still provide improvements in our current practices.

Acknowledgments. Collaboration on this project would not have been possible without travel support from the European Severe Storm Laboratory for the first author to attend the 10th European Conference on Severe Storms hosted in Kraków, Poland, in November 2019. We are grateful for the comments provided by Drs. Matthew Bunkers, Pieter Groenemeijer, and Aaron Kennedy and an anonymous reviewer, which improved this article. This work benefited from discussions and feedback from Andy Wade, Levi Lovell, and Nicholas Goldacker in the convective storms group at North Carolina State University. The authors thank John Hart, Ryan Jewell, Bryan Smith, and Rich Thompson of the NOAA/NWS Storm Prediction Center for their work on the underlying software used to generate the RUC/RAP SFCOA proximity sounding database, tireless effort in assigning convective modes to each report, and their generosity for sharing the data with the community. The European Severe Storms Laboratory is gratefully acknowledged for providing severe weather reports. Figure 1 was made in ESRI ArcMap. Figures 2, 5, and 9 were created using the Seaborn package in Python. Figures 3 and 8 were assisted via the Metpy package in Python (May et al. 2017). Figure 4 used the windrose package in Python, while Figs. 7 and 10 were created using the verif package in Python. The first two authors were supported by NSF AGS-1748715 and NOAA NA19OAR4590341. Taszarek was supported by grants from the Polish National Science Centre (2017/27/B/ST10/00297) and the Polish National Agency for Academic Exchange—The Bekker Programme (PPN/BEK/2018/1/00199).

REFERENCES

- Allen, J. T., and D. J. Karoly, 2014: A climatology of Australian severe thunderstorm environments 1979–2011: Inter-annual variability and ENSO influence. *Int. J. Climatol.*, 34, 81–97, https://doi.org/10.1002/joc.3667.
- Beebe, R. G., 1958: Tornado proximity soundings. *Bull. Amer. Meteor. Soc.*, **39**, 195–201, https://doi.org/10.1175/1520-0477-39.4.195.
- Bell, T. M., B. R. Greene, P. M. Klein, M. Carney, and P. B. Chilson, 2020: Confronting the boundary layer data gap: Evaluating new and existing methodologies of probing the lower atmosphere. *Atmos. Meas. Tech.*, 13, 3855–3872, https://doi.org/10.5194/amt-13-3855-2020.
- Benjamin, S. G., and Coauthors, 2004: An hourly assimilation-forecast cycle: The RUC. *Mon. Wea. Rev.*, **132**, 495–518, https://doi.org/10.1175/1520-0493(2004)132<0495:AHACTR> 2.0.CO;2.
- ——, and Coauthors, 2016: A North American hourly assimilation and model forecast cycle: The Rapid Refresh. *Mon. Wea. Rev.*, 144, 1669–1694, https://doi.org/10.1175/MWR-D-15-0242.1.

- Blair, S. F., and Coauthors, 2017: High-resolution hail observations: Implications for NWS warning operations. *Wea. Forecasting*, **32**, 1101–1119, https://doi.org/10.1175/WAF-D-16-0203.1.
- Bothwell, P., J. Hart, and R. Thompson, 2002: An integrated threedimensional objective analysis scheme in use at the Storm Prediction Center. 21st Conf. on Severe Local Storms, San Antonio, TX, Amer. Meteor. Soc., JP3.1, https://ams.confex.com/ ams/SLS_WAF_NWP/techprogram/paper_47482.htm.
- Brooks, H. E., 2009: Proximity soundings for severe convection for Europe and the United States from reanalysis data. *Atmos. Res.*, **93**, 546–553, https://doi.org/10.1016/j.atmosres.2008.10.005.
- —, and J. Correia Jr., 2018: Long-term performance metrics for National Weather Service tornado warnings. Wea. Forecasting, 33, 1501–1511, https://doi.org/10.1175/WAF-D-18-0120.1.
- —, C. A. Doswell III, and J. Cooper, 1994: On the environments of tornadic and nontornadic mesocyclones. *Wea. Forecasting*, 9, 606–618, https://doi.org/10.1175/1520-0434(1994)009<0606: OTEOTA>2.0.CO:2.
- Bunkers, M. J., 2018: Observations of right-moving supercell motion forecast errors. Wea. Forecasting, 33, 145–159, https://doi.org/10.1175/WAF-D-17-0133.1.
- ——, B. A. Klimowski, J. W. Zeitler, R. L. Thompson, and M. L. Weisman, 2000: Predicting supercell motion using a new hodograph technique. Wea. Forecasting, 15, 61–79, https://doi.org/10.1175/1520-0434(2000)015<0061:PSMUAN>2.0.CO;2.
- —, D. A. Barber, R. L. Thompson, R. Edwards, and J. Garner, 2014: Choosing a universal mean wind for supercell motion prediction. *J. Oper. Meteor.*, 2, 115–129, https://doi.org/ 10.15191/nwajom.2014.0211.
- Chilson, P. B., and Coauthors, 2019: Moving towards a network of autonomous UAS atmospheric profiling stations for observations in the earth's lower atmosphere: The 3D mesonet concept. *Sensors*, **19**, 2720, https://doi.org/10.3390/s19122720.
- Chisholm, A. J., and J. Renick, 1972: The kinematics of multicell and supercell Alberta hailstorms. Research Council of Alberta Hail Studies Rep. 72-2, 24-31.
- Clark, A. J., M. C. Coniglio, B. E. Coffer, G. Thompson, M. Xue, and F. Kong, 2015: Sensitivity of 24-h forecast dryline position and structure to boundary layer parameterizations in convection-allowing WRF model simulations. Wea. Forecasting, 30, 613–638, https://doi.org/10.1175/WAF-D-14-00078.1.
- Coffer, B. E., and M. D. Parker, 2017: Simulated supercells in nontornadic and tornadic VORTEX2 environments. *Mon. Wea. Rev.*, **145**, 149–180, https://doi.org/10.1175/MWR-D-16-0226.1.
- —, and ——, 2018: Is there a "tipping point" between simulated nontornadic and tornadic supercells in VORTEX2 environments? *Mon. Wea. Rev.*, **146**, 2667–2693, https://doi.org/ 10.1175/MWR-D-18-0050.1.
- —, —, J. M. Dahl, L. J. Wicker, and A. J. Clark, 2017: Volatility of tornadogenesis: An ensemble of simulated nontornadic and tornadic supercells in VORTEX2 environments. *Mon. Wea. Rev.*, **145**, 4605–4625, https://doi.org/10.1175/ MWR-D-17-0152.1.
- —, —, R. L. Thompson, B. T. Smith, and R. E. Jewell, 2019: Using near-ground storm relative helicity in supercell tornado forecasting. Wea. Forecasting, 34, 1417–1435, https://doi.org/ 10.1175/WAF-D-19-0115.1.
- Coniglio, M. C., 2012: Verification of RUC 0–1-h forecasts and SPC mesoscale analyses using VORTEX2 soundings. *Wea.*

- Forecasting, 27, 667–683, https://doi.org/10.1175/WAF-D-11-00096.1.
- —, and M. D. Parker, 2020: Insights into supercells and their environments from three decades of targeted radiosonde observations. *Mon. Wea. Rev.*, **148**, 4893–4915, https://doi.org/ 10.1175/MWR-D-20-0105.1.
- —, J. Correia Jr., P. T. Marsh, and F. Kong, 2013: Verification of convection-allowing WRF Model forecasts of the planetary boundary layer using sounding observations. *Wea. Forecasting*, 28, 842–862, https://doi.org/10.1175/WAF-D-12-00103.1.
- Craven, J. P., H. E. Brooks, and J. A. Hart, 2004: Baseline climatology of sounding derived parameters associated with deep, moist convection. *Natl. Wea. Dig.*, 28, 13–24.
- Davies, J. M., and R. H. Johns, 1993: Some wind and instability parameters associated with strong and violent tornadoes: 1. Wind shear and helicity. *The Tornado: Its Structure, Dynamics, Prediction, and Hazards, Geophys. Monogr.*, Vol. 79, Amer. Geophys. Union, 573–582.
- Davies-Jones, R., 1984: Streamwise vorticity: The origin of updraft rotation in supercell storms. *J. Atmos. Sci.*, **41**, 2991–3006, https://doi.org/10.1175/1520-0469(1984)041<2991:SVTOOU> 2.0.CO;2.
- Dennis, E. J., and M. R. Kumjian, 2017: The impact of vertical wind shear on hail growth in simulated supercells. *J. Atmos. Sci.*, **74**, 641–663, https://doi.org/10.1175/JAS-D-16-0066.1.
- Doswell, C. A., III, and D. M. Schultz, 2006: On the use of indices and parameters in forecasting severe storms. *Electron. J. Severe Storms Meteor.*, 1 (3), https://www.ejssm.org/ojs/index.php/ejssm/article/viewArticle/11/12.
- ——, R. Davies-Jones, and D. L. Keller, 1990: On summary measures of skill in rare event forecasting based on contingency tables. Wea. Forecasting, 5, 576–585, https://doi.org/10.1175/1520-0434(1990)005<0576:OSMOSI>2.0.CO;2.
- Dotzek, N., P. Groenemeijer, B. Feuerstein, and A. M. Holzer, 2009: Overview of ESSL's severe convective storms research using the European Severe Weather Database ESWD. Atmos. Res., 93, 575–586, https://doi.org/10.1016/ j.atmosres.2008.10.020.
- Esterheld, J. M., and D. J. Giuliano, 2008: Discriminating between tornadic and non-tornadic supercells: A new hodograph technique. *Electron. J. Severe Storms Meteor.*, **3** (2), https://www.ejssm.org/ojs/index.php/ejssm/article/viewArticle/33/37.
- Flournoy, M. D., M. C. Coniglio, E. N. Rasmussen, J. C. Furtado, and B. E. Coffer, 2020: Modes of storm-scale variability and tornado potential in VORTEX2 near- and far-field tornadic environments. *Mon. Wea. Rev.*, 148, 4185–4207, https://doi.org/10.1175/MWR-D-20-0147.1.
- Gensini, V. A., T. L. Mote, and H. E. Brooks, 2014: Severe-thunderstorm reanalysis environments and collocated radio-sonde observations. J. Appl. Meteor. Climatol., 53, 742–751, https://doi.org/10.1175/JAMC-D-13-0263.1.
- Groenemeijer, P., and T. Kühne, 2014: A climatology of tornadoes in Europe: Results from the European Severe Weather Database. Mon. Wea. Rev., 142, 4775–4790, https://doi.org/ 10.1175/MWR-D-14-00107.1.
- Hersbach, H., and Coauthors, 2020: The ERA5 global reanalysis. *Quart. J. Roy. Meteor. Soc.*, **146**, 1999–2049, https://doi.org/10.1002/qj.3803.
- Huuskonen, A., E. Saltikoff, and I. Holleman, 2014: The operational weather radar network in Europe. *Bull. Amer. Meteor. Soc.*, 95, 897–907, https://doi.org/10.1175/BAMS-D-12-00216.1.
- Johns, R. H., J. M. Davies, and P. W. Leftwich, 1993: Some wind and instability parameters associated with strong and violent

- tornadoes: 2. Variations in the combinations of wind and instability parameters. *The Tornado: Its Structure, Dynamics, Prediction, and Hazards, Geophys. Monogr.*, Vol. 79, Amer. Geophys. Union, 583–590.
- Kaltenböck, R., G. Diendorfer, and N. Dotzek, 2009: Evaluation of thunderstorm indices from ECMWF analyses, lightning data and severe storm reports. *Atmos. Res.*, 93, 381–396, https:// doi.org/10.1016/j.atmosres.2008.11.005.
- Kerr, B. W., and G. L. Darkow, 1996: Storm-relative winds and helicity in the tornadic thunderstorm environment. *Wea. Forecasting*, **11**, 489–505, https://doi.org/10.1175/1520-0434(1996) 011<0489:SRWAHI>2.0.CO;2.
- King, A. T., and A. D. Kennedy, 2019: North American supercell environments in atmospheric reanalyses and RUC-2. J. Appl. Meteor. Climatol., 58, 71–92, https://doi.org/10.1175/JAMC-D-18-0015.1.
- Kumjian, M. R., and K. Lombardo, 2020: A hail growth trajectory model for exploring the environmental controls on hail size: Model physics and idealized tests. *J. Atmos. Sci.*, 77, 2765– 2791, https://doi.org/10.1175/JAS-D-20-0016.1.
- LeCun, Y., Y. Bengio, and G. Hinton, 2015: Deep learning. *Nature*, **521**, 436–444, https://doi.org/10.1038/nature14539.
- Li, F., D. R. Chavas, K. A. Reed, I. Dawson, and T. Daniel, 2020: Climatology of severe local storm environments and synopticscale features over North America in ERA5 reanalysis and CAM6 simulation. *J. Climate*, 33, 8339–8365, https://doi.org/ 10.1175/JCLI-D-19-0986.1.
- Maddox, R. A., 1976: An evaluation of tornado proximity wind and stability data. *Mon. Wea. Rev.*, **104**, 133–142, https://doi.org/ 10.1175/1520-0493(1976)104<0133:AEOTPW>2.0.CO;2.
- Markowski, P. M., 2020: What is the intrinsic predictability of tornadic supercell thunderstorms? *Mon. Wea. Rev.*, 148, 3157– 3180, https://doi.org/10.1175/MWR-D-20-0076.1.
- —, J. M. Straka, and E. N. Rasmussen, 1998: A preliminary investigation of the importance of helicity location in the hodograph. 19th Conf. on Severe Local Storms, Minneapolis, MN, Amer. Meteor. Soc., 230–233.
- —, C. Hannon, J. Frame, E. Lancaster, A. Pietrycha, R. Edwards, and R. L. Thompson, 2003: Characteristics of vertical wind profiles near supercells obtained from the Rapid Update Cycle. Wea. Forecasting, 18, 1262–1272, https://doi.org/10.1175/1520-0434(2003)018<1262:COVWPN>2.0.CO;2.
- May, R., S. Arms, P. Marsh, E. Bruning, and J. Leeman, 2017: Metpy: A python package for meteorological data. Unidata, accessed 1 January 2020, https://doi.org/10.5065/D6WW7G29.
- McGovern, A., K. L. Elmore, D. J. Gagne, S. E. Haupt, C. D. Karstens, R. Lagerquist, T. Smith, and J. K. Williams, 2017: Using artificial intelligence to improve real-time decision-making for high-impact weather. *Bull. Amer. Meteor. Soc.*, 98, 2073–2090, https://doi.org/10.1175/BAMS-D-16-0123.1.
- Monteverdi, J. P., C. A. Doswell III, and G. S. Lipari, 2003: Shear parameter thresholds for forecasting tornadic thunderstorms in northern and central California. *Wea. Forecasting*, 18, 357–370, https://doi.org/10.1175/1520-0434(2003)018<0357: SPTFFT>2.0.CO;2.
- Nevius, D. S., and C. Evans, 2018: The influence of vertical advection discretization in the WRF-ARW model on capping inversion representation in warm-season, thunderstorm-supporting environments. Wea. Forecasting, 33, 1639–1660, https://doi.org/10.1175/WAF-D-18-0103.1.
- Parker, M. D., 2014: Composite VORTEX2 supercell environments from near-storm soundings. *Mon. Wea. Rev.*, 142, 508–529, https://doi.org/10.1175/MWR-D-13-00167.1.

- Peters, J. M., C. J. Nowotarski, and H. Morrison, 2019: The role of vertical wind shear in modulating maximum supercell updraft velocities. *J. Atmos. Sci.*, 76, 3169–3189, https://doi.org/ 10.1175/JAS-D-19-0096.1.
- Púčik, T., P. Groenemeijer, D. Rýva, and M. Kolář, 2015: Proximity soundings of severe and nonsevere thunderstorms in central Europe. *Mon. Wea. Rev.*, 143, 4805–4821, https://doi.org/10.1175/MWR-D-15-0104.1.
- Rasmussen, E. N., 2003: Refined supercell and tornado forecast parameters. *Wea. Forecasting*, **18**, 530–535, https://doi.org/10.1175/1520-0434(2003)18<530:RSATFP>2.0.CO;2.
- —, and D. O. Blanchard, 1998: A baseline climatology of sounding-derived supercell and tornado forecast parameters. Wea. Forecasting, 13, 1148–1164, https://doi.org/10.1175/1520-0434(1998)013<1148:ABCOSD>2.0.CO;2.
- Rodríguez, O., and J. Bech, 2018: Sounding-derived parameters associated with tornadic storms in Catalonia. *Int. J. Climatol.*, **38**, 2400–2414, https://doi.org/10.1002/joc.5343.
- Roebber, P. J., 2009: Visualizing multiple measures of forecast quality. Wea. Forecasting, 24, 601–608, https://doi.org/10.1175/ 2008WAF2222159.1.
- Saltikoff, E., and Coauthors, 2019: OPERA the radar project. *Atmosphere*, **10**, 320, https://doi.org/10.3390/atmos10060320.
- Schaefer, J. T., and R. L. Livingston, 1988: The typical structure of tornado proximity soundings. J. Geophys. Res., 93, 5351–5364, https://doi.org/10.1029/JD093iD05p05351.
- Sherburn, K. D., and M. D. Parker, 2014: Climatology and ingredients of significant severe convection in high-shear, low-CAPE environments. Wea. Forecasting, 29, 854–877, https://doi.org/10.1175/WAF-D-13-00041.1.
- —, and —, 2019: The development of severe vortices within simulated high-shear, low-CAPE convection. *Mon. Wea. Rev.*, **147**, 2189–2216, https://doi.org/10.1175/MWR-D-18-0246.1.
- —, —, J. R. King, and G. M. Lackmann, 2016: Composite environments of severe and nonsevere high-shear, low-CAPE convective events. *Wea. Forecasting*, 31, 1899–1927, https://doi.org/10.1175/WAF-D-16-0086.1.
- Smith, B. T., R. L. Thompson, J. S. Grams, C. Broyles, and H. E. Brooks, 2012: Convective modes for significant severe thunderstorms in the contiguous United States. Part I: Storm classification and climatology. Wea. Forecasting, 27, 1114–1135, https://doi.org/10.1175/WAF-D-11-00115.1.
- Stull, R. B., 1988: An Introduction to Boundary Layer Meteorology. Kluwer Academic, 666 pp.
- Taszarek, M., H. E. Brooks, and B. Czernecki, 2017: Sounding-derived parameters associated with convective hazards in Europe. *Mon. Wea. Rev.*, 145, 1511–1528, https://doi.org/10.1175/MWR-D-16-0384.1.
- —, —, —, P. Szuster, and K. Fortuniak, 2018: Climatological aspects of convective parameters over Europe: A comparison of ERA-Interim and sounding data. *J. Climate*, 31, 4281–4308, https://doi.org/10.1175/JCLI-D-17-0596.1.

- —, and Coauthors, 2019: A climatology of thunderstorms across Europe from a synthesis of multiple data sources. *J. Climate*, 32, 1813–1837, https://doi.org/10.1175/JCLI-D-18-0372.1.
- —, J. T. Allen, H. E. Brooks, N. Pilguj, and B. Czernecki, 2020a: Differing trends in United States and European severe thunderstorm environments in a warming climate. *Bull. Amer. Meteor. Soc.*, https://doi.org/10.1175/BAMS-D-20-0004.1, in press.
- —, T. Púčik, K. A. Hoogewind, and H. E. Brooks, 2020b: Severe convective storms across Europe and the United States. Part II: ERA5 environments associated with lightning, large hail, severe wind, and tornadoes. *J. Climate*, **33**, 10263–10286, https://doi.org/10.1175/JCLI-D-20-0346.1.
- Thompson, R. L., 1998: Eta model storm-relative winds associated with tornadic and nontornadic supercells. *Wea. Forecasting*, **13**, 125–137, https://doi.org/10.1175/1520-0434(1998)013<0125: EMSRWA>2.0.CO;2.
- —, R. Edwards, J. A. Hart, K. L. Elmore, and P. Markowski, 2003: Close proximity soundings within supercell environments obtained from the Rapid Update Cycle. Wea. Forecasting, 18, 1243–1261, https://doi.org/10.1175/1520-0434(2003)018<1243:CPSWSE>2.0.CO;2.
- —, C. M. Mead, and R. Edwards, 2007: Effective storm-relative helicity and bulk shear in supercell thunderstorm environments. Wea. Forecasting, 22, 102–115, https://doi.org/10.1175/WAF969.1.
- ——, B. T. Smith, J. S. Grams, A. R. Dean, and C. Broyles, 2012: Convective modes for significant severe thunderstorms in the contiguous United States. Part II: Supercell and QLCS tornado environments. Wea. Forecasting, 27, 1136–1154, https:// doi.org/10.1175/WAF-D-11-00116.1.
- Wade, A. R., M. C. Coniglio, and C. L. Ziegler, 2018: Comparison of near-and far-field supercell inflow environments using radiosonde observations. *Mon. Wea. Rev.*, 146, 2403–2415, https://doi.org/10.1175/MWR-D-17-0276.1.
- Warren, R. A., H. Richter, H. A. Ramsay, S. T. Siems, and M. J. Manton, 2017: Impact of variations in upper-level shear on simulated supercells. *Mon. Wea. Rev.*, 145, 2659–2681, https:// doi.org/10.1175/MWR-D-16-0412.1.
- Weisman, M. L., and J. B. Klemp, 1982: The dependence of numerically simulated convective storms on vertical wind shear and buoyancy. *Mon. Wea. Rev.*, **110**, 504–520, https://doi.org/10.1175/1520-0493(1982)110<0504:TDONSC>2.0.CO;2.
- ——, and R. Rotunno, 2000: The use of vertical wind shear versus helicity in interpreting supercell dynamics. *J. Atmos. Sci.*, **57**, 1452–1472, https://doi.org/10.1175/1520-0469(2000)057<1452: TUOVWS>2.0.CO;2.
- Wilks, D. S., 2011: Statistical Methods in the Atmospheric Sciences.
 3rd ed. International Geophysics Series, Vol. 100, Academic Press, 704 pp.
- Wurman, J., D. Dowell, Y. Richardson, P. Markowski, E. Rasmussen, D. Burgess, L. Wicker, and H. B. Bluestein, 2012: The second Verification of the Origins of Rotation in Tornadoes Experiment: VORTEX2. *Bull. Amer. Meteor. Soc.*, 93, 1147–1170, https://doi.org/10.1175/BAMS-D-11-00010.1.